Cooling-rate effects in amorphous silica: A computer-simulation study

Katharina Vollmayr,* Walter Kob,† and Kurt Binder
Institut für Physik, Johannes Gutenberg-Universität, Staudinger Weg 7, D-55099 Mainz, Germany
(Received 24 June 1996; revised manuscript 26 August 1996)

Using molecular-dynamics computer simulations we investigate how in silica the glass transition and the properties of the resulting glass depend on the cooling rate with which the sample is cooled. By coupling the system to a heat bath with temperature $T_b(t)$, we cool the system linearly in time, $T_b(t)=T_i-\gamma t$, where γ is the cooling rate. In qualitative accordance with experiments, the temperature dependence of the density shows a local maximum, which becomes more pronounced with decreasing cooling rate. We find that the glass transition temperature T_g is in accordance with a logarithmic dependence on γ. The enthalpy, density, and thermal expansion coefficient for the glass at zero temperature decrease with decreasing γ. We show that also microscopic quantities, such as the radial distribution function, the bond-bond angle distribution function, the coordination numbers, and the distribution function for the size of the rings, depend significantly on γ. We demonstrate that the cooling-rate dependence of these microscopic quantities is significantly more pronounced than the one of macroscopic properties. Furthermore, we show that these microscopic quantities, as determined from our simulation, are in good agreement with the ones measured in real experiments, thus demonstrating that the used potential is a good model for silica glass. The vibrational spectrum of the system also shows a significant dependence on the cooling rate and is in qualitative accordance with the one found in experiments. Finally we investigate the properties of the system at finite temperatures in order to understand the microscopic mechanism for the density anomaly. We show that the anomaly is related to a densification and subsequent opening of the tetrahedral network when the temperature is decreased, whereas the distance between nearest neighbors, i.e., the size of the tetrahedra, does not change significantly. [S0163-1829(96)03946-X]

I. INTRODUCTION

The last few years have shown that computer simulations are a very effective tool to gain insight into the structure and dynamics of supercooled liquids and glasses and that they are therefore a very useful extension of experimental and analytical investigations of such systems.[1–3] The main reason for the success of such simulations is based upon two facts: First, that they allow one to investigate the structure of such systems in full microscopic detail and, second, that for most *atomic* systems many interesting dynamical phenomena occur on a time scale that is accessible to such simulations, i.e., happen between 10^{-12} and 10^{-7} s. It is this time range on which much of the recent investigations on the dynamics of supercooled liquids has been focused, since many of the predictions of the so-called mode-coupling theory, a theory that attempts to describe the dynamics of supercooled liquids,[4] can be tested well in this time window.

If in a supercooled liquid the temperature is decreased so much that the relaxation times of the system exceed the time scale of the experiment or of the computer simulation, the system will fall out of equilibrium and undergo a glass transition, provided that it does not crystallize. Thus the resulting glass is a nonequilibrium structure and its properties will in general depend on its history of production such as, e.g., the rate with which the sample was cooled or compressed. Such dependences have indeed been found in experiments and in computer simulations. For example, it has been demonstrated in experiments[5–8] and in computer simulations[9–14] that the density or the glass transition temperature depends on the cooling rate. In some of these simulations also more microscopic quantities, such as the radial distribution function or the radius of gyration of polymers, have been investigated and it was shown that also these quantities depend on the cooling rate.[11,13,14] In particular it was shown that certain microscopic quantities show a much stronger dependence on the cooling rate than macroscopic quantities (e.g., in Refs. 13 and 14) which shows that it might be interesting to extend the experiments in this direction also.

An important difference between computer simulations of supercooled liquids and of glasses should be pointed out. In the former type of studies one investigates the *equilibrium* properties of the system. Thus a direct comparison between the results from simulations and experiments is possible. This is not the case for glasses, which are *nonequilibrium* systems. As mentioned in the previous paragraph, the temperature at which the system undergoes a glass transition will depend on the time scale of the experiment. Since the time scales of the computer simulation are many orders of magnitude shorter than the ones of a typical laboratory experiment, it follows that the glass transition temperature on the computer is significantly higher than the glass transition temperature one observes in the laboratory (assuming all other things to be equal). (An exception are experiments with ion bombardment of glasses in which the cooling rates become comparable to the ones used in computer simulations.[15]) Thus, if the properties of glasses are investigated by computer simulations, it is necessary to see how these properties depend on the way the glass was produced before a comparison with real experiments can be made. Such a check is of particular importance if one is interested in the microscopic properties of the glass since, as we have mentioned above, these quantities usually show a stronger dependence of the production history than the macroscopic properties.

The goal of the present paper is twofold. On the one hand, we want to investigate how the cooling rate affects the microscopic properties of a *strong* glass former and compare these dependences with the results of a similar simulation we did for a *fragile* glass former.[12–14] Second, we want to investigate whether the two-body potential that was recently proposed by van Beest, Kramer, and van Santen[16] (BKS) for the description of *crystalline* silica is able to reproduce also structural properties of *amorphous* silica. Apart from being of great importance in chemistry, geology, and industrial applications, silica is also a prototype of a network-forming glass and thus it has been investigated extensively.[17–27] Since the BKS potential contains only two-body terms, it can be implemented in a simulation much more efficiently than a potential which contains also three-body terms. This in turn allows one to make longer runs and thus to study the equilibrium properties of the system at lower temperatures or to investigate glasses which have a lower glass transition temperature and are therefore more realistic.

The rest of the paper is organized as follows. In the next section we give the details of the used potential as well as of the simulation. Section III contains the results and consists of three parts: In the first one we study the properties of the system *during* the cooling procedure and therefore the glass transition. In the second part we investigate how the properties of the glass depend on the cooling rate with which it was produced, i.e., *after* having been cooled to zero temperature. The third subsection is then devoted to investigate the system at *finite* temperatures in order to relate the properties of the system in its glass phase to the ones at finite temperature. In the last section we then summarize and discuss the results.

II. MODEL AND DETAILS OF THE SIMULATION

As already mentioned in the Introduction, silica is a very important glass former and thus there have been many investigations in which this system has been studied by means of computer simulations. Thus it is not surprising that there are many different types of potentials in use which seem to be able to give a more or less realistic description of the real potential. One of the most successful is the so-called BKS potential, proposed by van Beest, Kramer, and van Santen a few years ago.[16] Is was shown that this potential is able to give a good description of the various crystalline phases of silica.[28] It is therefore interesting to see how well it is able to describe the amorphous phase as well. One of the appealing features of this potential is that it contains only two-body terms, thus avoiding the three-body terms that are present in some other potentials for silica, making the BKS potential very attractive for computer simulations.

The functional form of the BKS potential is given by a sum of a Coulomb term, an exponential, and a van der Waals term. Thus the potential between particle i and j is given by

$$\phi(r_{ij})=\frac{q_i q_j e^2}{r_{ij}}+A_{ij}e^{-B_{ij}r_{ij}}-\frac{C_{ij}}{r_{ij}^6}, \tag{1}$$

where e is the charge of an electron and the constants A_{ij}, B_{ij}, and C_{ij} are given by $A_{\mathrm{SiSi}}=0.0$ eV, $A_{\mathrm{SiO}}=18\,003.7572$ eV, $A_{\mathrm{OO}}=1388.7730$ eV, $B_{\mathrm{SiSi}}=0.0$ Å^{-1}, $B_{\mathrm{SiO}}=4.873\,18$ Å^{-1}, $B_{\mathrm{OO}}=2.760\,00$ Å^{-1}, $C_{\mathrm{SiSi}}=0.0$ eV Å^{-6}, $C_{\mathrm{SiO}}=133.5381$ eV Å^{-6}, and $C_{\mathrm{OO}}=175.0000$ eV Å^{-6}.[16] The partial charges q_i are $q_{\mathrm{Si}}=2.4$ and $q_{\mathrm{O}}=-1.2$ and e^2 is given by $1602.19/(4\pi 8.8542)$ eV Å. The so-defined potentials for the Si-O and O-O interactions have the unphysical property of diverging to minus infinity at small distances. However, this is not a severe drawback, since in order to get to these small distances the particles have to overcome a barrier which is, e.g., in the case of the Si-O interaction, on the order of 5000 K. In our simulations we have observed that even at a temperature of 7000 K the particles are relatively unlikely to cross this barrier, thus indicating that the *effective* barrier is probably even larger than 5000 K. In order to prevent, in the rare cases in which the particles cross the barrier, the particles from fusing together, we have substituted the potential given by Eq. (1) by a harmonic potential when r_{ij} is smaller than the location of the barrier, i.e., for $r_{ij}\leqslant 1.1936$ Å and $r_{ij}\leqslant 1.439$ Å in the case of the Si-O and O-O interactions. Note that for intermediate and low temperatures this modification does not affect the potential given by Eq. (1) and that in this limit we are thus working with the usual BKS potential.

The Coulomb interaction was computed by using the Ewald method[18,29] with a constant, α/L of 6.5, where L is the size of the cubic box, and by using all q vectors with $|q|\leqslant 6\times 2\pi/L$. In order to save computer time the non-Coulombic contribution to the potential was truncated and shifted at a distance of 5.5 Å. Note that this truncation is not negligible since it affects the pressure of the system. We will comment on this point more when we discuss the temperature dependence of the density. In order to minimize surface effects periodic boundary conditions were used. The masses of the Si and O atoms were 28.086 and 15.9994 u, respectively. The number of particles was 1002, of which 334 were silica atoms and 668 were oxygen atoms.

Our simulations were done at constant pressure ($p_{\mathrm{ext}}=0$), thus allowing us to compute the temperature dependence of the density and the specific heat at constant pressure and hence to compare our results with real experiments. For this we used the algorithm proposed by Andersen[30] with the mass of the piston set to 4×10^{-3} u for the equilibration of the system and to 1×10^{-3} u for the production. The equations of motion were integrated with the velocity form of the Verlet algorithm. The step size was 1.6 fs which was sufficiently small to allow us to neglect the drift in the enthalpy of the system when the thermostat was not active. This thermostat was a stochastic collision procedure which periodically substituted the velocities of all the particles with those drawn from a Boltzmann distribution that corresponded to the temperature of the heat bath. For the equilibration we coupled the system at every 50 time steps to a stochastic heat bath and propagated it in the (NPT) ensemble at a temperature of 7000 K for about 32 000 time steps. After this time the configuration and velocities were saved for the subsequent quenching procedure. Then the equilibration run at $T_b=7000$ K was continued for another 40 000 steps and the resulting configuration saved. These 40 000 time steps were long enough to completely decorrelate the system at this temperature. This process was repeated until we had 20 configurations at $T_b=7000$ K which were completely uncorrelated.

In order to simulate the cooling process we took these

configurations as a starting point of a constant pressure run in which T_b, the temperature of the heat bath, was decreased linearly in time t, i.e., $T_b(t)=T_i-\gamma t$. Here T_i is the initial temperature ($=7000$ K) and γ is the cooling rate. The system was coupled to this heat bath every 150 time steps and between these stochastic collisions it was propagated in the (NPH) ensemble, where H is the enthalpy. This cooling process was continued until the temperature of the heat bath was zero, i.e., for a time T_i/γ. The so-obtained configuration was subsequently relaxed with respect to the coordinates of the particles and the volume of the system to its nearest metastable state in configuration space. For the sake of efficiency this relaxation was done with a multidimensional conjugate gradient method.[31] An equivalent alternative would have been to continue the molecular-dynamics (MD) simulation at $T_b=0$ for a very long time. The so-obtained final configurations were then analyzed in order to investigate how the so-produced glass depends on the cooling rate.

The cooling rates investigated were 1.14×10^{15}, 5.68×10^{14}, 2.84×10^{14}, 1.42×10^{14}, 7.10×10^{13}, 3.55×10^{13}, 1.77×10^{13}, 8.87×10^{12}, and 4.44×10^{12} K/s. Although these cooling rates are of course many orders of magnitude larger than the ones used in the laboratory, it is currently not possible to simulate a quench of the system with cooling rates that are significantly smaller than the ones used here, since for the smallest cooling rate the length of the runs was about 10^6 MD steps which took about 340 h of CPU time on a IBM-RS6000/370.

We also mention that the range of cooling rates investigated here is about a factor of 10 smaller than the one we used in a similar investigation on a binary Lennard-Jones mixture.[12–14] The reason for this is that for the Lennard-Jones system the potential is short ranged whereas the long-range potential needed for silica [Eq. (1)] slows down the computation of the forces by about a factor of 30.

In order to improve the statistics of the results it was necessary to average for each cooling rate over several independent runs. For most values of γ we averaged over ten independent starting configurations which were obtained as described above. An exception were $\gamma=7.10\times10^{13}$ K/s and $\gamma=3.55\times10^{13}$ K/s for which we averaged over 20 configurations.

III. RESULTS

This section consists of three subsections. In the first one we investigate the properties of the system during the cooling from high temperatures to zero temperatures, and how the occurring glass transition depends on the cooling rate. In the second subsection we study how the properties of the glass at zero temperatures depend on the cooling rate. In the third subsection we use the information that we gained in the first two subsections to understand better the microscopic structure of silica at finite temperatures.

A. Cooling-rate dependence of the quench

One of the simplest quantities one can study in a cooling process is the enthalpy H of the system which is given by $H=E_{\rm kin}+E_{\rm pot}+M\dot{V}^2/2+p_{\rm ext}V$, where $E_{\rm kin}$ and $E_{\rm pot}$ are the kinetic and potential energy of the system, respectively, and

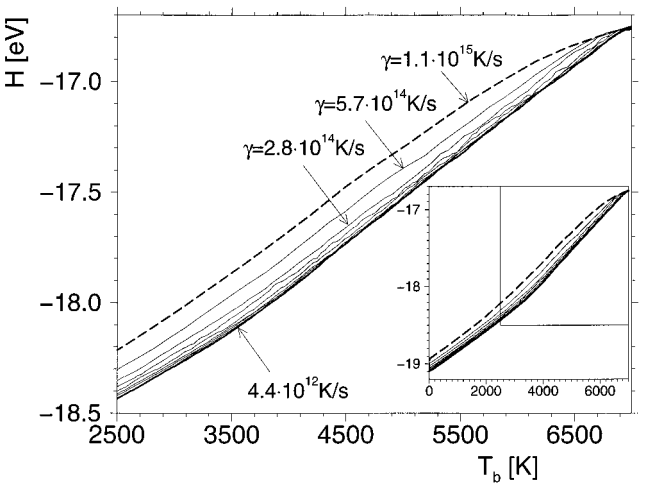

FIG. 1. Enthalpy H of the system vs T_b, the temperature of the heat bath, for all cooling rates investigated. Main figure: enlargement of the glass transition region. The solid and dashed bold curves are the smallest and largest cooling rates, respectively. Inset: full range of temperature.

M, V, and $p_{\rm ext}$ are the mass of the piston, the volume of the system, and the external pressure. Earlier simulations of glass-forming systems have shown that $H(T_b)$ has a noticeable bend when the temperature is lowered from high temperatures to low temperatures. It is assumed that at the temperature at which this bend occurs the system falls out of equilibrium, because the typical relaxation times of the system exceed the time scale of the cooling process. Therefore this temperature can be identified with the glass transition temperature T_g.

In Fig. 1 we show the enthalpy of the system as a function of the temperature of the heat bath for all cooling rates investigated. The inset shows the whole range of temperature and we see that the curves show the mentioned bend at a temperature around 3500 K. This is thus the temperature range in which the system falls out of equilibrium for the cooling rates investigated. This temperature range is shown enlarged in the main figure. We now see that there is a clear dependence of $H(T_b)$ on the cooling rate in that the curves corresponding to the large cooling rates are higher than the ones for the small cooling rates. At high temperatures the curves for intermediate and small cooling rates fall on top of each other to within the noise of the data, which means that for these temperatures and cooling rates the system has not yet fallen out of equilibrium. Only at lower temperatures do the curves for the intermediate values of the cooling rate split off from this equilibrium (liquidus) curve and thus is the system starting to undergo a glass transition and we see that the temperature at which this happens decreases with decreasing cooling rate. Also note that for the largest cooling rates this splitting off happens at the starting temperature, thus indicating that for such large cooling rates the system falls out of equilibrium immediately.

In order to determine the cooling rate dependence of the temperature at which the system undergoes its glass transition we use the concept of the ''fictive temperature'' as introduced by Tool and Eichlin. [32] This concept makes use of the observation that at high temperatures the curves for not

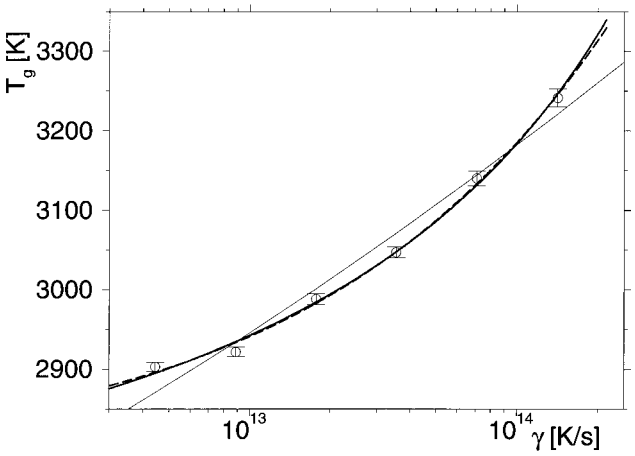

FIG. 2. Glass transition temperature T_g vs the cooling rate. The solid line is a fit with the functional form given by Eq. (2), the dashed line with a power law, and the thin solid line with an Arrhenius law.

too large cooling rates fall onto a master curve and that at low temperatures the curves have the same form, i.e., can be collapsed onto a master curve by shifting them *vertically*. The intersection of the extrapolation of these two master curves gives then an estimate for the glass transition temperature T_g. We therefore fitted the curves for $\gamma \leqslant 3.55\times 10^{13}$ K/s in the temperature range 5000 K $\leqslant T_b \leqslant$ 6750 K with a straight line and did the same with the curves for $\gamma \leqslant 1.42\times 10^{14}$ K/s in the low-temperature range 0 $\leqslant T_b \leqslant$ 1250 K. Note that the determination of the glass temperature via the mentioned procedure is only reasonable if the high-temperature part of the curve actually falls onto the liquidus curve. Since this is not the case for the three fastest cooling rates, we have not determined T_g for these cooling rates.

In Fig. 2 we show the so-determined glass transition temperature as a function of the cooling rate. We see that a variation of γ by about 1.5 decades gives rise to a variation of T_g of about 350 K. Also included in the figure is a fit to the data with the functional form

$$T_g(\gamma) = T_0 - \frac{B}{\ln(\gamma A)} \tag{2}$$

(solid line), which is obtained by assuming a Vogel-Fulcher dependence of the relaxation time τ of the system on the temperature, i.e., $\tau(T) = A \exp[B/(T-T_0)]$, and arguing that the system falls out of equilibrium at that temperature at which the relaxation time is on the order of the time scale of the cooling process, i.e., $\tau(T_g) = \gamma^{-1}$.[1,33] We see that this type of fit describes the data very well, as is the case in real experiments.[7] For the parameters A and B we find 1.8×10^{-16} s/K and 2625 K, respectively. The Vogel temperature T_0, i.e., the glass temperature that would be observed upon an infinitesimal cooling rate, is 2525 K, which is significantly higher than the experimental value of 1446 K.[34] (Here we assume that for the cooling rates used in the laboratory the dependence of T_g on the cooling rate is sufficiently small, so that we can use the results of experiments at a finite cooling rate as a good approximation for T_0.) Thus we come to the conclusion that either the extrapolation of the cooling rate dependence as given in Eq. (2) is not correct, because we are not yet in the range of cooling rates where Eq. (2) holds, or that the silica model studied here does not reproduce well the glass transition temperature.

We also mention that further sources of uncertainty in the determination of T_0 are finite-size effects in the simulation. Such dependences have indeed been observed in experiments with relatively simple liquids[35] and also a recent computer simulation of silica has shown that the relaxation behavior of such a system is severely affected by finite-size effects.[36]

In a similar study on cooling-rate effects in a Lennard-Jones glass[14] we have found that the dependence of T_g on the cooling rate is also fitted well by the function $T_g(\gamma) = T_c + (A\gamma)^{1/\delta}$, which follows from the assumption that the temperature dependence of the relaxation time is given by $\tau(T) = A(T-T_c)^{-\delta}$, a functional form that is suggested by the so-called mode-coupling theory of the glass transition.[4] We therefore tried to fit our data for the γ dependence of T_g also in the present case with this functional form and found that it is also able to describe the data well (with $T_c = 2778$ K and $\delta = 2.52$) (dashed line in Fig. 2). Thus, if the two functional forms are merely seen as fitting functions, they can be considered as equally good. Furthermore, we have also tried to fit the data with an Arrhenius law, the functional form that seems to describe well the experimental data. (Note that Rössler and Sokolov have recently demonstrated that the viscosity of silica at temperatures a bit above T_g shows a non-Arrhenius behavior,[37] but this range of viscosity is outside the range of our simulation.) The result of this type of fit is included in the figure as well (thin solid line) and is clearly inferior to the two other functional forms. Thus it seems that the relaxation times of silica show at high temperatures a qualitative different temperature dependence than at low temperatures, which is analogous to the dependence found in water,[38] a network former that is in many aspects similar to silica.

As stated above, we observe a change of T_g of about 300 K when the cooling rate is varied by 1.5 decades. Such a change in T_g is significantly larger than the values measured in real experiments in which this quantity was determined for various materials.[5,7,8] It is found that a variation of the cooling rate by one decade gives rise to a change of T_g on the order of 10 K, thus much less than the 300 K determined here. The reason for this discrepancy is probably the huge difference between the cooling rates used in the simulation and the one used in the laboratory. If we use the parameters from our fit to T_g and extrapolate this $T_g(\gamma)$ dependence to a laboratory cooling rate of 0.1 K/s, we find that the predicted change of T_g is only about 5 K per decade of cooling rate, which is in good agreement with the typical values found in experiments.[5,7,8]

By differentiating the enthalpy with respect to the temperature T_b, we obtain c_p, the specific heat at constant pressure. Since the original data were a bit too noisy to allow for a direct differentiation, we parametrized $H(T_b)$ with a spline under tension[39] and differentiated this spline. Figure 3 shows the resulting specific heat for all cooling rates investigated. To facilitate the comparison with experimental values we have chosen the units of c_p to be J/g K. From this figure we see that at high temperatures the fastest cooling rates show a strong increase with decreasing temperature. The reason for

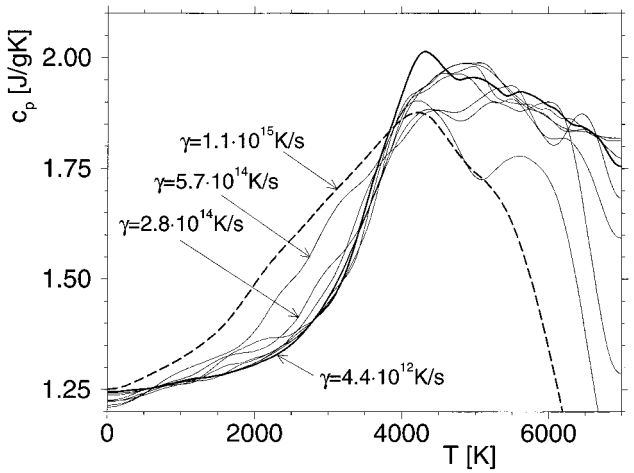

FIG. 3. Specific heat vs T_b for all cooling rates investigated. The solid and dashed bold curves are the smallest and largest cooling rates, respectively.

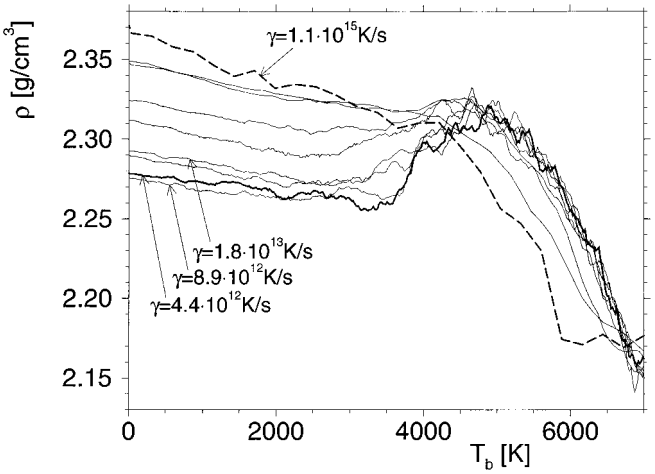

FIG. 4. Density of the system vs T_b for all cooling rates investigated. The solid and dashed bold curves are the smallest and largest cooling rates, respectively. Note the presence of a local maximum in ρ at temperatures around 4800 K if γ is small.

this is that for these fast cooling rates the system falls out of equilibrium already at the start of the quench (see Fig. 1), thus giving rise to this increase of c_p. After this increase c_p attains a maximum of about 1.85 J/g K at a temperature around 4200 K and then drops again to a value of 1.25 J/g K for $T_b=0$.

The real equilibrium curve of c_p at high temperatures is given by the curves for slow cooling rates. We see that c_p increases slowly from a value around 1.80 J/g K to a value around 1.95 J/g K when the temperature is decreased from 7000 to 4300 K. At this latter temperature the specific heat starts to drop quickly, indicating that the system undergoes the glass transition, and attains a value around 1.25 J/g K at $T_b=0$ K. This value is close to the classical Dulong-Petit value of 1.236 J/g K expected for a harmonic solid. We notice that in the temperature range where the glass transition takes place the temperature dependence of c_p is independent of the cooling rate to within the accuracy of our data, if the cooling rate is not too large. This is in contrast to our findings for the previously investigated Lennard-Jones system,[14] for which we found that the drop in c_p at the glass transition becomes steeper with decreasing cooling rate. Since we have seen a clear cooling rate dependence of the temperature dependence of the enthalpy (see Fig. 1), it can be concluded that its derivative, i.e., c_p, should show a cooling rate dependence also and that thus the reason for our failure to detect one must be given by the statistical inaccuracy of our data.

Since neither the low- nor high-temperature dependence of c_p shows a strong dependence on the cooling rate, if γ is not too large, we can compare the values of c_p above and below the glass transition temperature with their experimental counterparts. Brückner reports that around 1500 K the value of c_p for amorphous silica is about 1.23 J/g K,[40] which compares well with the one found in this simulation, i.e., 1.25 J/g K. At a temperature of 2000 K Brückner gives the value 1.50 J/g K, which is significantly less than the one found in our simulation ($c_p \approx 1.8$ J/g K at $T_b=7000$ K). Thus we see that the here-used BKS potential does not give an accurate description of the magnitude of the jump in the specific heat. One possible reason for the observed discrepancy might, however, not be the inadequacy of the potential, but the fact that the Debye temperature of silica is relatively high [1200 K, (Ref. 40)] thus showing that quantum effects might be important even at the temperatures we are considering.

We now turn our attention to a further important macroscopic quantity, the density ρ. In Fig. 4 we show ρ as a function of the bath temperature T_b for all cooling rates investigated. As in the case of the enthalpy we find that at high temperatures the curves for all but the three fastest cooling rates fall onto a master curve, the equilibrium curve. From the curves corresponding to small cooling rates we recognize that this equilibrium curve shows a maximum at around 4800 K. Thus we find that, in accordance with experiments,[40–42] this model shows an anomaly in the density. The experimental value for the temperature of the maximum in ρ is 1820 K, thus significantly lower than the temperature at which we observe the anomaly. Since we see that, within the accuracy of our data, the temperature at which this anomaly occurs is independent of the cooling rate, we conclude that for the BKS potential this anomaly is indeed at a temperature which is too high, even if one would cool the system with a significantly smaller cooling rate. It has to be mentioned, however, that for different potentials this anomaly occurs at even higher temperatures or is not present at all,[19] thus showing that with respect to this feature the BKS potential is superior to other potentials.

For intermediate and small values of γ the value of ρ decreases after having passed through the maximum. At even lower temperatures the curves then start to increase again. The temperature at which this increasing trend starts decreases with decreasing cooling rate, thus showing that the curves follow the low-temperature side of the hump the longer the smaller the cooling rate is. At even lower temperatures the curves become, within the accuracy of our data, straight lines with negative slope.

From Fig. 4 we also recognize that, in the temperature range considered, the relative change in density is relatively small (less than 10%) which is in accordance with the experimental finding that the thermal expansion coefficient of

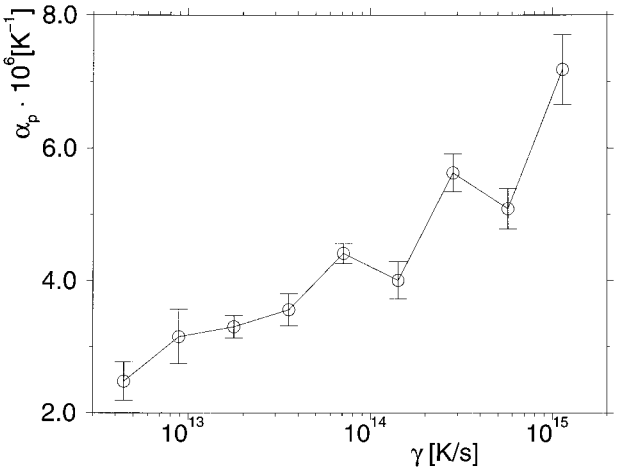

FIG. 5. Thermal expansion coefficient at $T=0$ K vs cooling rate.

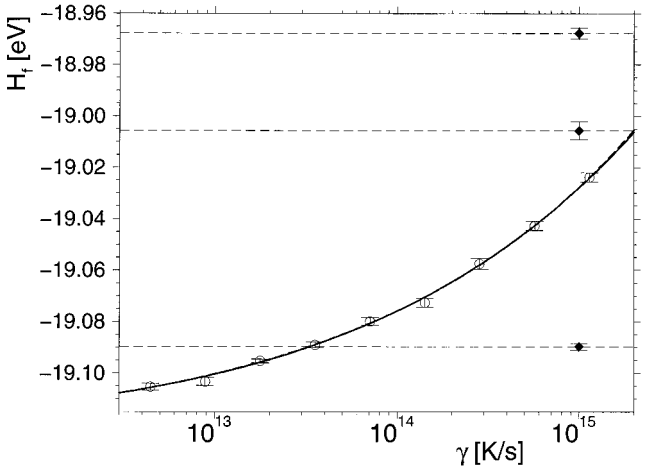

FIG. 6. Enthalpy after the quench vs the cooling rate (open circles). The solid and dashed curves are fits with the functional forms given by Eqs. (4) and (5), respectively. The three horizontal lines are the value of the enthalpy of the relaxed configuration at $T_b=7000$ K, $T_b=4840$ K, and $T_b=3220$ K (top to bottom). See text for details.

silica is small.[41,45] We also note that at low temperatures the density is around 2.3 g/cm^3, which compares well with experiments.[41,43] It is interesting that a simulation with the *original* BKS potential, i.e., without the cutoff at 5.5 Å (see Sec. II), gave at 5000 K a density of 2.6 g/cm^3, thus about 10% higher than the one found in this work.[44] This shows how sensitively quantities like the pressure depend on the details of the potential at large distances. Since the introduction of the cutoff moves the value of the density closer to the experimental one, we thus find that this cutoff gives rise to a more realistic description of amorphous silica.

From the temperature dependence of the density we can extract

$$\alpha_p = \frac{1}{V}\frac{\partial V}{\partial T}\bigg|_p = -\frac{1}{\rho}\frac{\partial \rho}{\partial T}\bigg|_p , \tag{3}$$

the thermal expansion coefficient at constant pressure. We determined α_p at $T=0$ K from the slope of the straight line of $\rho(T)$ at low temperatures (see Fig. 4). The resulting cooling rate dependence of $\alpha_p(T=0\ \mathrm{K})$ is shown in Fig. 5. We recognize that this quantity shows a decreasing trend with decreasing cooling rate and that, within the accuracy of our data, it is not possible to say what the asymptotic value for very small cooling rates is. However, the experimental value of α_p, 5.5×10^{-7} K/s,[41,45] is certainly compatible with an extrapolation of our data to $\gamma=0$.

It is also interesting to compare this result with the one found in a similar investigation of a binary Lennard-Jones system,[14] where *no* significant dependence of α_p at $T=0$ K on the cooling rate was found. Since a nonzero α_p is the result of the anharmonicity of the local potential, we thus come to the conclusion that in this model for silica these anharmonic effects are cooling rate dependent, whereas they are not for the Lennard-Jones system, i.e., for a prototype of a simple liquid.

B. Cooling-rate dependence of the properties of the glass

In the previous subsection we investigated how the cooling rate affects macroscopic quantities like the enthalpy or the density at *finite* temperatures. The goal of the present subsection is to see how the cooling rate affects various macroscopic and microscopic quantities of the glass at $T=0$ K, i.e., of the final product of the quench and the subsequent relaxation of the system as described above.

The first quantity we investigate is the value of the enthalpy of the glass at $T=0$ K. In Fig. 1 we have seen that at finite temperatures the curves of the enthalpy $H(T_b)$ follow the equilibrium curve as long as the relaxation time of the system is smaller than the time scale of the cooling process, i.e., γ^{-1}. If the two time scales become comparable, the system undergoes a glass transition and the curves for $H(T_b)$ remain *above* the equilibrium curve. Therefore we expect that the final value of the enthalpy decreases with decreasing γ. That this is indeed the case is shown in Fig. 6 where we show H_f, the value of the enthalpy after the quench, for all cooling rates investigated.

From a formal point of view the cooling process can also be seen as an optimization problem in which the system tries to minimize the enthalpy. It will manage to do this the better the more time it is given to search for this minimum. Thus one might ask what the value of the enthalpy (the cost function) is when the system is given a certain amount of time, characterized here by the cooling rate, to minimize H. Such types of questions have been addressed already in other types of complex optimization problems and also for other types of glass formers.[46–48] From theoretical arguments one can expect the cost function to show either a logarithmic or a power-law dependence on the cooling rate,[47] i.e.,

$$H_f(\gamma) = H_f^0 + a_1(-\ln\gamma)^{a_2} \tag{4}$$

or

$$H_f(\gamma) = H_f^0 + b_1\gamma^{b_2}, \tag{5}$$

where H_f^0, a_i, and b_i are fit parameters. We therefore fitted our data for H_f with the two functional forms and the result of these fits is included in Fig. 6 as well. We recognize that,

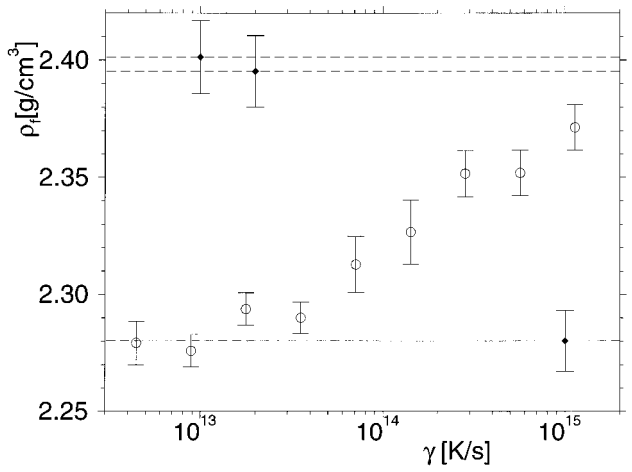

FIG. 7. Density after the quench vs the cooling rate. The three horizontal lines are the value of the density of the relaxed configuration at $T_b = 7000$ K, $T_b = 4840$ K, and $T_b = 3220$ K (top to bottom). See text for details.

in the cooling range investigated, both functional forms fit the data equally well. The values we obtain for H_f^0 are -19.1213 eV for the logarithmic dependence and -19.1252 eV for the power-law dependence. With the accuracy of our data we are not able to decide which functional form, if any, is appropriate to describe our data. This is the same conclusion we came to in case of the earlier-mentioned investigation of a Lennard-Jones system.[14]

Next we turn our attention to the cooling rate dependence of the density. In Fig. 7 we show the density of the glass after the quench versus the cooling rate. The densities we found for the glass are between 2.27 and 2.38 g/cm^3 which compares well with the experimental values of 2.2 g/cm^3.[41,43] We see that, contrary to most real glasses or Lennard-Jones systems,[5,8,14] ρ_f *decreases* with decreasing cooling rate, a behavior that can be understood by remembering our observation (see Fig. 4) that for small cooling rates the curves for the density follow the equilibrium curve also when the latter is decreasing on the low-temperature side of the density anomaly. It should be noted, however, that this observed decrease of the final density with decreasing cooling rate cannot be the correct asymptotic behavior for very small cooling rate. The reason for this is that we know that at low temperatures the thermal expansion coefficient of silica is positive [as can be seen in experiments or from the fact that the density decreases with increasing temperature (see Fig. 4)]. Thus we expect that the equilibrium curve for the density will, after having shown a decreasing behavior for temperatures just below the density anomaly, bend upward again. If a quench is made with a very small, but finite, value of γ, the corresponding curve for the density will fall out of equilibrium in that temperature range where the equilibrium curve will already show the *increasing* behavior (with decreasing temperature). Therefore the final density of the glass as produced with such a small cooling rate will be *lower* than the one which would be obtained with an infinitesimal small cooling rate; i.e., at very small cooling rate the curve $\rho_f(\gamma)$ will increase with decreasing cooling rate. Thus we conclude that the cooling rate dependence of ρ_f as seen in Fig. 7 is not yet the asymptotic one. Hence it

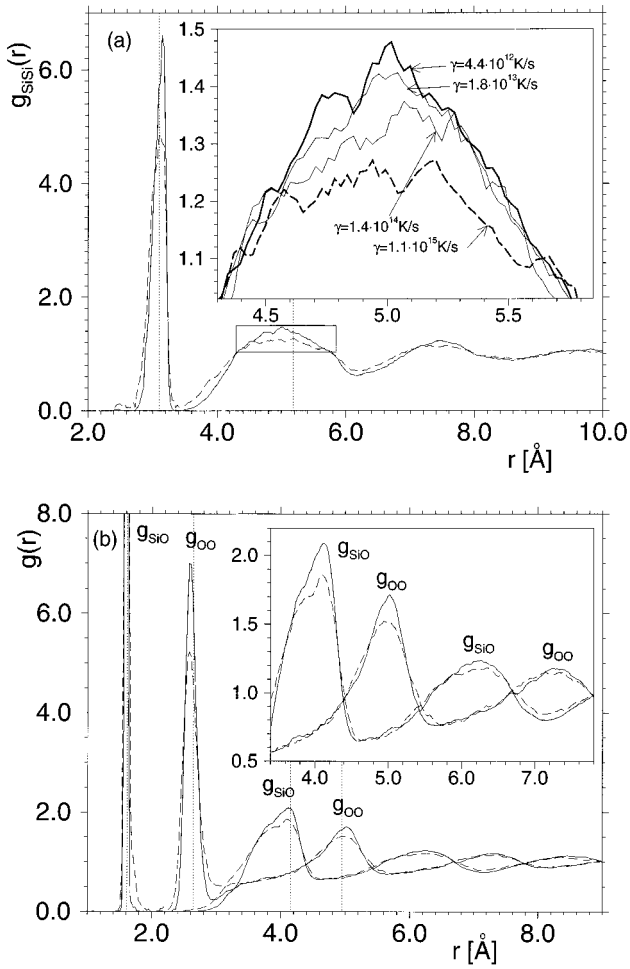

FIG. 8. Radial distribution function. (a) $g_{\mathrm{SiSi}}(r)$. Main figure: the slowest (solid curve) and fastest (dashed curve) cooling rate. The vertical dotted lines give the position of the peaks as determined from experiments (see Table I). Inset: enlargement of the second-nearest-neighbor peak for four selected cooling rates. (b) $g_{\mathrm{SiO}}(r)$ and $g_{\mathrm{OO}}(r)$ for the slowest (solid curves) and fastest (dashed curve) cooling rate. Inset: enlargement of the second- and third-nearest-neighbor peak.

does not make sense to use one of the formulas given in Eqs. (4) and (5) to extrapolate $\rho_f(\gamma)$ to very small cooling rates.

After having presented our results on the cooling rate dependence of the macroscopic properties of the glass we now turn our attention to the microscopic properties of the system in order to gain some understanding about how the macroscopic behavior is related to the microscopic one.

The first quantity we investigate is the radial distribution function $g_{\alpha\beta}(r)$ between species α and β ($\alpha,\beta \in \{\mathrm{Si,O}\}$).[49] This function allows one to see how the structure of the glass changes on the various length scales when the cooling rate is changed. In Fig. 8(a) we show $g_{\mathrm{SiSi}}(r)$ for the largest and smallest cooling rate investigated (main figure), as well as an enlargement of the region of the second-nearest-neighbor peak for a few selected cooling rates (inset). From the main figure we recognize that with decreasing cooling rate the structural order at short and intermediate distances (i.e., $r \lesssim 8$ Å) increases, in that the peaks and minima become more pronounced. In particular we see that the height of the first-nearest-neighbor peak changes by

TABLE I. Location of the first- and second-nearest-neighbor peaks in the radial distribution function $g(r)$. The numbers in parentheses in the second column give the error in units of the last digit.

		Simulation [Å]	Experiment [Å]	
SiO	first peak	1.595(5)	1.608[b]	1.620[a]
	second peak	4.12(1)		4.15[a]
OO	first peak	2.590(5)	2.626[b]	2.65[a]
	second peak	5.01(2)		4.95[a]
SiSi	first peak	3.155(10)	3.077[c]	3.12[a]
	second peak	5.05(5)		5.18[a]

[a]Reference 43.
[b]Reference 50.
[c]Reference 51.

about 20%. The amount of this change is significantly larger than any change we observed for macroscopic properties, thus showing that the microscopic properties can show a much stronger dependence on the cooling rate than the macroscopic properties do.

In Fig. 8(b) we show the radial distribution function for the Si-O and the O-O pairs for the largest and smallest cooling rate investigated. Also in this case we notice a significant cooling-rate dependence for distances $r \leqslant 8$ Å, i.e., the short- and medium-range order are affected significantly by the cooling rate in that the order increases with decreasing cooling rate.

From the curves presented in Fig. 8 we see that, although the *height* of the various peaks shows a significant dependence on the cooling rate, the *location* of the peaks is affected much less by a variation of γ. Thus it is reasonable to compare the location of these peaks with the ones as determined in experiments. In Table I we give the location of the nearest- and second-nearest-neighbor peaks as well as the corresponding experimental values (also included in Fig. 8 as vertical dotted lines). The locations of these peaks were determined from the data for the slowest cooling rate. We see that, although the accordance between experiment and the results of our simulation is not perfect, the BKS potential does quite well to reproduce the short- and medium-range structure of the glass and can therefore, from this point of view, be considered as a good model also for amorphous silica.

Having investigated the cooling-rate dependence of the radial distribution function we now move on to study how the structure factor $S(q)$ depends on γ. Although from a mathematical point of view the radial distribution function and the structure factor contain the same information, the importance of the latter for scattering experiments makes it worthwhile to investigate its cooling-rate dependence as well. In Fig. 9 we thus show the three partial structure factors. We recognize from these figures that the $S(q)$ show a significant dependence on the cooling rate for small and intermediate values of q, in that the height of the main peak as well as the so-called first sharp diffraction peak (FSDP), i.e., the peak to the left of the main peak, depend on γ. This FSDP has recently been the focus of significant interest, since it characterizes the stucture of the glass on intermediate length scales and its microscopic origin is still a matter of debate.[52] In the case of the Si-Si and Si-O correlations the corresponding structure factors show only a weak dependence on γ for q values larger than the location of the main peak. For the case of the O-O correlation, however, even for large values of q a noticeable dependence of $S(q)$ on γ is observed, indicating that the short-range order of O-O pairs

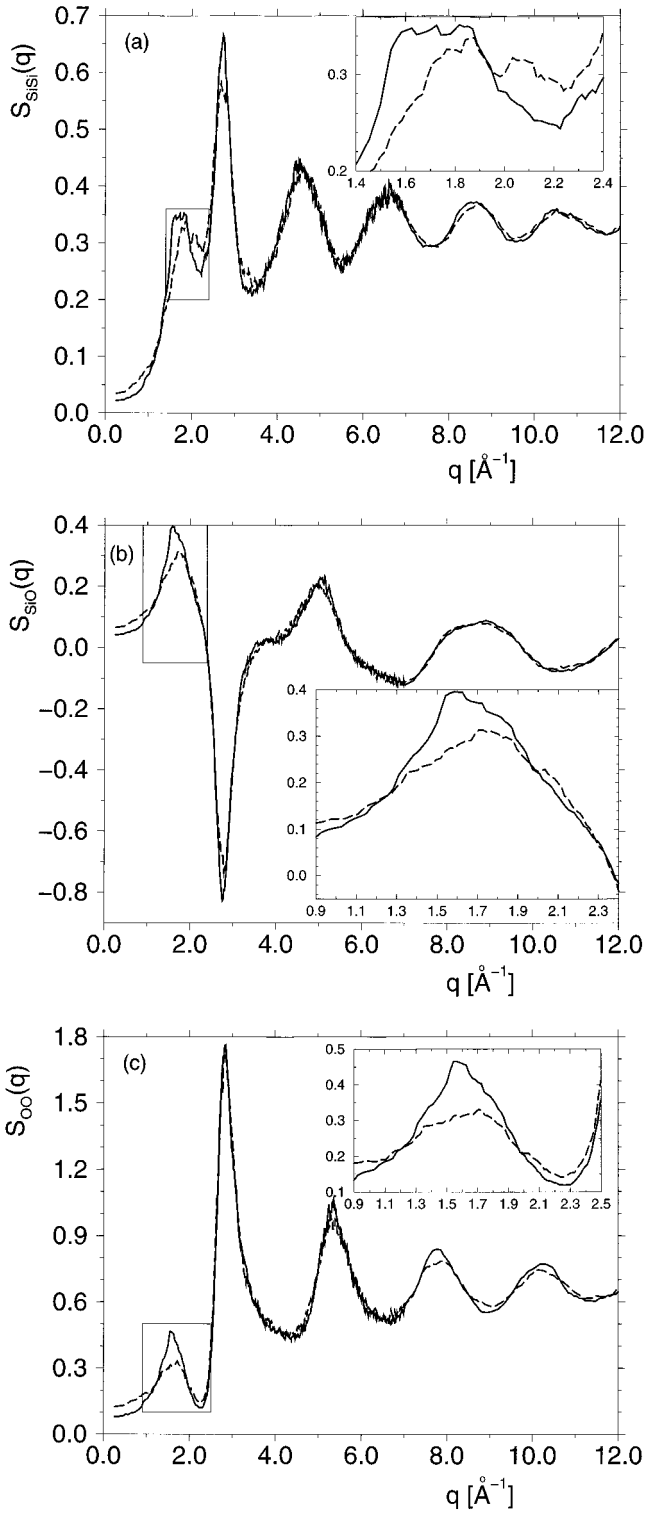

FIG. 9. Partial structure factors for the slowest (solid curve) and fastest (dashed curve) cooling rate. Insets: enlargement of the first sharp diffraction peak. (a) Si-Si correlation. (b) Si-O correlation. (c) O-O correlation.

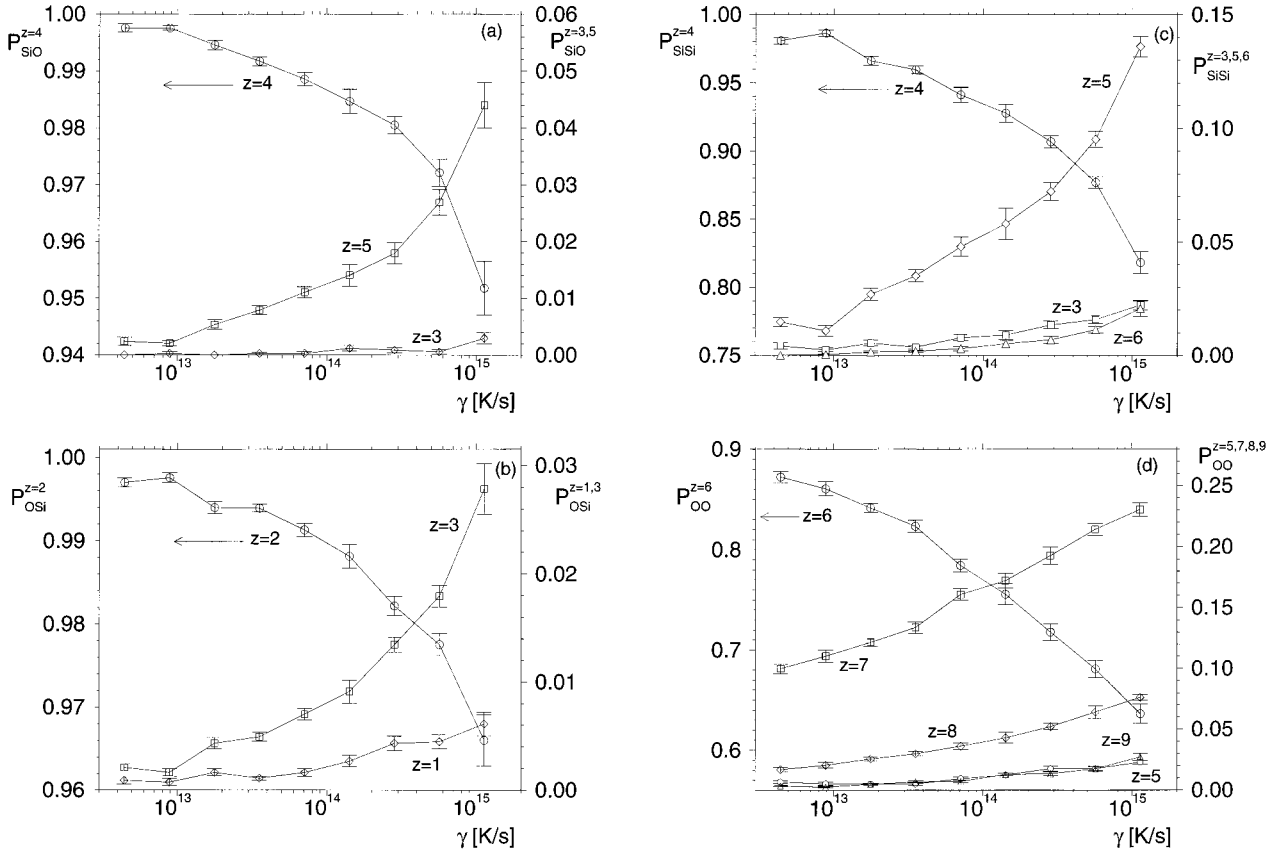

FIG. 10. Partial coordination numbers vs the cooling rate. (a) Si-O pairs. (b) O-Si pairs. (c) Si-Si pairs. (d) O-O pairs. Note the different scales for the various curves.

changes significantly. The main change in the structure of $S(q)$ occurs, however, in all three correlation function for values of q close to the FSDP (see insets). We see that the cooling rate affects this peak in two ways in that its height as well its position is changed. Since this peak reflects the medium-range order of the system, we thus come to the conclusion that the structure of the glass on these length scales is significantly affected by the cooling rate.

From the knowledge of $r_{\min}$, the location of the first minimum in the radial distribution function, we can compute the (partial) coordination number z of particle i, which we define as the number of other particles j with $|\mathbf{r}_j-\mathbf{r}_i|<r_{\min}$. We have found that $r_{\min}$ is essentially independent of the cooling rate and therefore we will use in the following always the same values, i.e., $r_{\min}^{\mathrm{SiSi}}=3.42$ Å, $r_{\min}^{\mathrm{SiO}}=2.20$ Å, and $r_{\min}^{\mathrm{OO}}=3.00$ Å. In Fig. 10 we show $P_{\alpha\beta}^{z=n}$ the probability that a particle of type α has n nearest neighbors of type β, versus the cooling rate γ.

First we study the nearest-neighbor pairs, i.e., the Si-O and the O-Si pairs [Figs. 10(a) and 10(b)]. We see that the vast majority of the silicon atoms is surrounded by four oxygen atoms, which can be understood by taking into account that at low pressures silica forms a network of corner-sharing tetrahedra, each of which has a silicon atom in its center and four oxygen atoms at its corners. The number of silica atoms that are not fourfold coordinated is about 5% for the fastest cooling rate and diminishes quickly to less than 0.5% when the cooling rate is decreased. This shows that the local order of the network, i.e., the frequency of tetrahedra, increases fast with decreasing cooling rate. The silicon atoms that are not fourfold coordinated are surrounded in most cases by five oxygen atoms and only a very small fraction is surrounded by three oxygen atoms. Figure 10(b) shows that most of the oxygen atoms are surrounded by two silicon atoms, also this observation in accordance with the above-mentioned network structure of corner-sharing tetrahedra. The number of oxygen atoms that are not twofold coordinated is for all cooling rates less than 3% and decreases quickly to less than 0.5% with decreasing γ. Thus we find that for slow cooling rates the BKS potential automatically gives the ''rules'' commonly postulated for ideal amorphous silica, namely, that this system is a ''continuous random network.''[53]

The just studied Si-O and O-Si coordination numbers are characteristic for the structure of the network on the *shortest* length scale. The coordination numbers for the Si-Si and the O-O pairs, however, are sensitive on a length scale of the structure that is a bit larger. In Figs. 10(c) and 10(d) we show the cooling-rate dependence of these coordination numbers. We see that most silicon atoms are surrounded by four other silicon atoms, although at the fastest cooling rate about 18% of them have a different Si-Si coordination number. This number shows that most tetrahedra are surrounded by four other tetrahedra, each of which has a silicon atom in its center. (See below for a further discussion of this point.) The curves for the O-O coordination numbers show that the most likely configuration is that an oxygen atom has six other oxygen atoms within a distance of $r_{\min}^{\mathrm{OO}}$ and that this probability increases significantly with decreasing cooling rate.

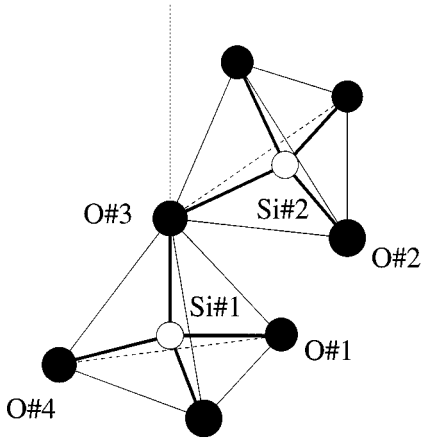

FIG. 11. Schematic representation of two corner-sharing tetrahedra.

These six oxygen atoms are the ones that sit in the corners of the two tetrahedra which are connected by the first oxygen atom (see Fig. 11). Thus we come also in this case to the conclusion that the order within the network increases with decreasing cooling rate.

Since we have just seen that the most frequent coordination number for the Si-Si and the O-O pairs can be rationalized by assuming that the network is composed of corner-sharing tetrahedra, we now investigate whether this argument is valid only on a qualitative basis or whether it is correct even on a quantitative basis. Thus the question is whether the cooling-rate dependence of the various coordination numbers for the Si-Si and the O-O pairs can be computed from the knowledge of the cooling-rate dependence of the coordination numbers of the Si-O and the O-Si pairs. In order to decide this we assumed that the coordination numbers for the Si-O are statistically independent from the ones of the O-Si pairs. If we postulate that a silicon atom that is a nearest neighbor of an oxygen atom will have a distance less than $r_{\min}^{\mathrm{SiSi}}$ from all other silicon atoms that are also nearest neighbors of this oxygen atom, it is relatively simple to compute the probability how many silicon atoms have a distance less than $r_{\min}^{\mathrm{SiSi}}$ from any given silicon atom. Using similar postulates for the other combinations of particles one can, e.g., show that within this ansatz the quantity $P_{\mathrm{SiSi}}^{z=4}$ is given by

$$P_{\mathrm{SiSi}}^{z=4}=P_{\mathrm{SiO}}^{z=3}[3P_{\mathrm{OSi}}^{z=1}(P_{\mathrm{OSi}}^{z=3})^2+3(P_{\mathrm{OSi}}^{z=2})^2P_{\mathrm{OSi}}^{z=3}]+P_{\mathrm{SiO}}^{z=4}[6(P_{\mathrm{OSi}}^{z=1})^2(P_{\mathrm{OSi}}^{z=3})^2+4(P_{\mathrm{OSi}}^{z=2})^4+12P_{\mathrm{OSi}}^{z=1}(P_{\mathrm{OSi}}^{z=2})^2P_{\mathrm{OSi}}^{z=3}]$$
$$+P_{\mathrm{SiO}}^{z=5}[5P_{\mathrm{OSi}}^{z=1}(P_{\mathrm{OSi}}^{z=2})^4+30(P_{\mathrm{OSi}}^{z=1})^2(P_{\mathrm{OSi}}^{z=2})^2P_{\mathrm{OSi}}^{z=3}+10(P_{\mathrm{OSi}}^{z=1})^3(P_{\mathrm{OSi}}^{z=3})^2]. \quad (6)$$

Similar expressions hold for the other values of the coordination numbers shown in Figs. 10(c) and 10(d). Equipped with these functions we now can compare the prediction of this factorization approximation with the measured values for the coordination numbers. In Fig. 12 we show the difference between the actual value of the coordination numbers and the predicted ones, i.e., $P_{\mathrm{sim}}^{z}-P_{\mathrm{appr}}^{z}$. We recognize from Fig. 12(a), that for the Si-Si pairs this factorization approximation is very good in that the difference between the actual values and the predicted one is less than 1.5% for fast cooling rates and is essentially zero, to within the statistical accuracy of our data, for small cooling rates. Thus we find that this factorization approximation works very well for the Si-Si pairs.

This agreement between the real data and the factorization approximation is not as good for the case of the O-O pairs [Fig. 12(b)]. We see that the discrepancy can be as large as 25% for the fastest cooling rate but that it diminishes, however, to less than 13% for the slowest cooling rate. The reason that the factorization approximation does not work as well in this case as it did in the case of the Si-Si pairs is likely to be the fact that two corner-sharing tetrahedra are tilted towards each other; i.e., the angle between silicon atom No. 1, bridging oxygen atom No. 3, and silicon atom No. 2 (see Fig. 11) is significantly less than 180°. Therefore oxygen atom No. 2 is also quite close to oxygen atom No. 1, although the former is, from a topological point of view, quite far away from the latter. Therefore it is not unlikely that oxygen atom No. 1 will have more than just six nearest-neighbor oxygen atoms. This is confirmed by the curve $P_{\mathrm{OO}}^{z=7}$ [see Fig. 10(d)], which shows that for fast cooling rates more than 20% of the oxygen atoms have more than six other oxygen atoms as nearest neighbors, and that this figure does not drop below 10% even in the case of the slowest cooling rate. That the tetrahedra actually have the local arrangement suggested above can be inferred from the bond-bond angles between neighboring atoms and therefore we will investigate this quantity next.

We have seen in Fig. 8 that the nearest-neighbor distance between silicon and oxygen atoms is essentially independent of the cooling rate. Thus we conclude that the tetrahedra do not change their size significantly when the cooling rate is varied. However, since we have found that the density of the system depends on the cooling rate, it must therefore be the case that it is the *relative arrangement* of neighboring tetrahedra which changes with γ. One possibility to characterize this relative arrangement is to consider the various bond-bond angles between the different atoms. In Fig. 13 we show the cooling-rate dependence of the distribution function for some selected angles for various cooling rates. Figure 13(a) shows this distribution function for the tetrahedral angle O-Si-O for all cooling rates investigated. For a perfect tetrahedra this angle is 109.47°. We see that P_{OSiO} has indeed a maximum close to this ideal angle. The location of this maximum is not quite the one of the ideal tetrahedron but with decreasing cooling rate it approaches this value. A decreasing cooling rate also leads to an increase of the height of the peak as well as a decrease of its width. Thus we find that the

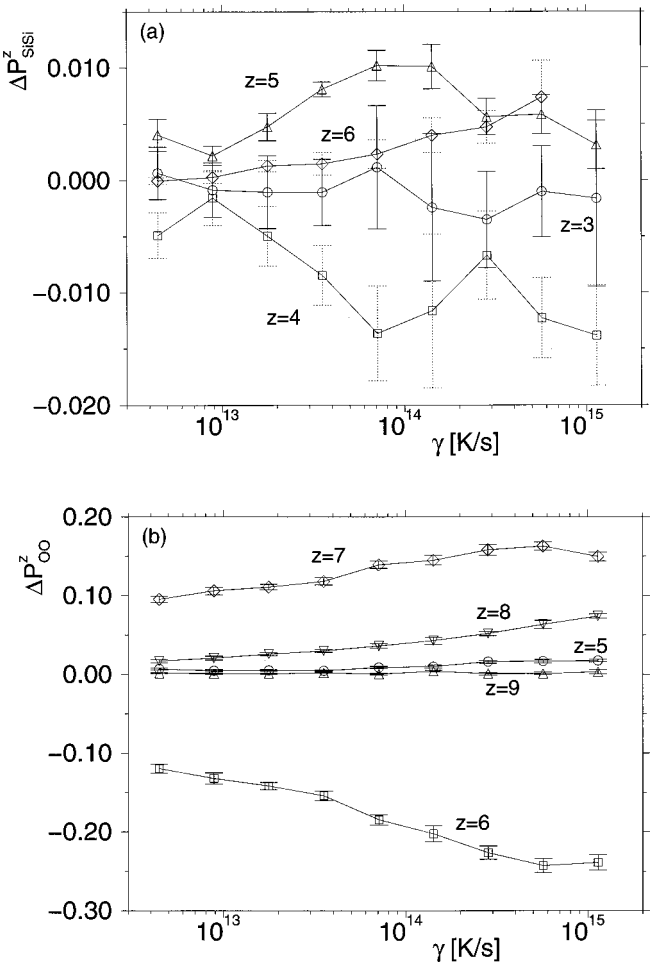

FIG. 12. Difference between the partial coordination numbers and the prediction of the factorization approximation. (a) Si-Si pairs. (b) O-O pairs.

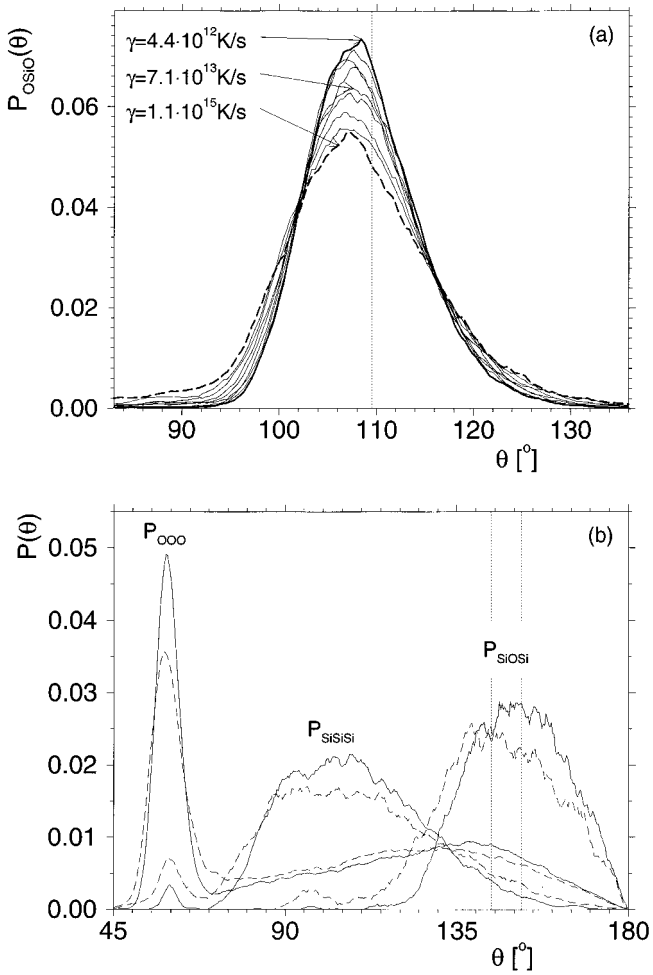

FIG. 13. Distribution function of various angles and cooling rates. (a) Angle O-Si-O for all cooling rates investigated. The bold solid and dashed curves correspond to the slowest and fastest cooling rates, respectively. The vertical line is the experimental value from Refs. 43, 55, and 56. (b) Angles O-O-O, Si-Si-Si, and Si-O-Si for the slowest (solid curves) and fastest (dashed curves) cooling rates investigated. The vertical lines are the experimental values from Refs. 43, 54, and 56.

structure of the local tetrahedra approaches indeed the one of an ideal tetrahedron when the cooling rate is decreased. The position of this peak is also in good agreement with the position found in experiments, as can be seen from Table II.

In Fig. 13(b) we show the distribution function for the angle between three neighboring oxygen atoms, P_{OOO}, for the fastest and slowest cooling rate investigated (dashed and solid curve, respectively). We see that P_{OOO} has two peaks. The first one is relatively sharp and has its maximum around 60°. It corresponds to the angle that is formed by three oxygen atoms of the same tetrahedron (e.g., O#1-O#3-O#4 in Fig. 11). With decreasing cooling rate this peak becomes significantly higher and narrower, indicating that the tetrahedra become more regular. The second peak is much broader than the first one and is located at around 135°. Its position changes from around 128° for fast cooling rates to around 137° for slow cooling rates. This peak corresponds to angles that are formed by an oxygen, on one tetrahedron, a bridging oxygen, and a third oxygen on the second tetrahedron (e.g., O#1-O#3-O#2 in Fig. 11). (Note that this angle is not only sensitive to the relative position of the two tetrahedra, i.e., the angle Si#1-O#3-Si#2, but also to their relative orientation. If the upper tetrahedron in Fig. 11 is rotated around the axis given by O#3-Si#2, the mentioned angle between the three O atoms will change also. This is probably the reason why the second peak is so broad.) The fact that this angle widens with decreasing cooling rate shows that the two neighboring tetrahedra move away from each other, thus making the structure less dense. Thus this mechanism is presumably the reason for the decrease in density after the density anomaly (see Fig. 4). We will investigate this point more in Sec. III C .

The picture of an opening network with decreasing cooling rate is also corroborated by the distribution of the Si-O-Si angle which is included in Fig. 13(b) also. We see that for fast cooling rates this distribution shows a large peak at 141° whose position moves to 152° for the smallest cooling rate, thus indicating that the network is opening up. From Table II we recognize that at the smallest cooling rate the location and the width of the peak are in fair agreement with the experimental values.

The angles O-Si-O, O-O-O, and Si-O-Si measure the angles between particles that are located on one or two tet-

TABLE II. Location and, in parentheses, the full width at half maximum of the angles O-Si-O and Si-O-Si as determined from the simulation and experiments.

	Simulation	Experiment			
	$\gamma = 4.4 \times 10^{12}$ K/s	Ref. 43	Ref. 54	Ref. 55	Ref. 56
OSiO	108.3° (12.8°)	109.5°		109.7°	109.4°
SiOSi	152° (35.7°)	144° (38)°	142° (26°)	144°, 152°	153°

rahedra. The fourth angle we consider, Si-Si-Si, is, however, defined by three particles that are in the center of *three* tetrahedra. Thus this angle is sensitive to the structure of the network on a length scale which is a bit larger. In Fig. 13(b) be show the distribution function for this angle as well. We see that this distribution shows a small peak at about 60° and a large peak between 90° and 120° which seems to be composed of at least two, possibly even three, peaks. The small peak at 60° was also observed by Rino *et al.*[20] and in that paper it was shown that such an angle occurs when the rings in the network (defined below) have length 4. Since such short rings occur relatively seldom (see below), also the corresponding peak is small. We also see that the height of this peak decreases significantly with decreasing cooling rate, which is in accordance with the observation discussed below that the number of rings of length 4 decreases with decreasing cooling rate. Also the main peak shows a noticeable dependence on γ in that its height increases and its width decreases with decreasing γ. Because, as mentioned above, this angle characterizes the structure of the network on an intermediate length scale, it is difficult to draw conclusions about the nature of this structure from the cooling-rate dependence of this distribution and thus we do not attempt to do it at this point.

A different way to characterize the structure of a network on the intermediate length scale is to consider the distribution of the frequency of rings of a given size. A ring is defined as follows: Starting from a Si atom one chooses two different O atoms that are nearest neighbors. Pick one of these. In general this O atom will also be a nearest neighbor of a second Si atom. From this new Si atom one then picks a new nearest-neighbor O atom, etc. This process is continued until one returns to the O atom which is the second one of the nearest-neighbor O atoms of the first Si atom. In this way one has constructed a closed loop of Si-O segments. The shortest one of these loops is called the ring associated with the original Si atom and the two nearest-neighbor O atoms. The number of Si-O segments in this loop is called the size of this ring. Both the distribution with which the so-defined rings occur and the distances and bond angles present in these rings were studied extensively in the paper by Rino *et al.*[20] Therefore we restrict ourselves at this place to study the cooling rate distribution of the size of the rings.

In Fig. 14 we show the probability that a particle is a member of a ring with a given size versus the cooling rate. Note that this distribution is not the same as the probability to find a ring of size n, since the two distributions differ by a weighting factor of n. A discussion of the latter distribution is given in Ref. 26. From Fig. 14 we recognize that for all cooling rates investigated rings of size 6 are the most frequent ones. This fact can be understood by considering the phase diagram of silica. At zero pressure the crystalline phase that is obtained when the system is cooled from the liquid phase is β-cristobalite,[57] which has only rings of size 6. (When the temperature is decreased even further one enters the phase of β-tridymite and then β-quartz, which have rings of size 6 and 8.) It can be expected that the *local* structure of the amorphous network will be similar to the crystalline network next to the liquid phase. We thus expect that also in the amorphous phase rings of size 6 are the most frequent ones and Fig. 14 shows that this is indeed the case.

From the figure we also recognize that very short and very long rings occur only seldom and that their frequency diminishes with decreasing cooling rate. [Note that we also found very few rings (less than 0.5%) of size 2 and 9, which are not shown in the figure.] Thus we find that also the distribution of the size of the rings, a quantity which characterizes the structure of the network on the intermediate length scale, depends noticeably on the cooling rate and that this dependence shows that the structure becomes more ordered, i.e., approaches the local topology of cristobalite, when the cooling rate is lowered.

The last quantity we investigate with respect to its cooling-rate dependence is the spectrum of the system. This quantity is interesting for two reasons: First it can be compared with the results of experiments and thus it provides a further test on how realistic the potential is and second it is also of general interest to study the spectrum in order to gain insight into the dynamical behavior of glasses at low temperatures.[14,21,58–62]

The spectrum was determined by computing the eigenvalues of the dynamical matrix given by $(m_j m_k)^{1/2} \partial^2 V(\{\mathbf{r}_i\}) / \partial r_{j,\alpha} \partial r_{k,\beta}$, where j and k are particle indices and α and β are the Cartesian components x,y,z. In

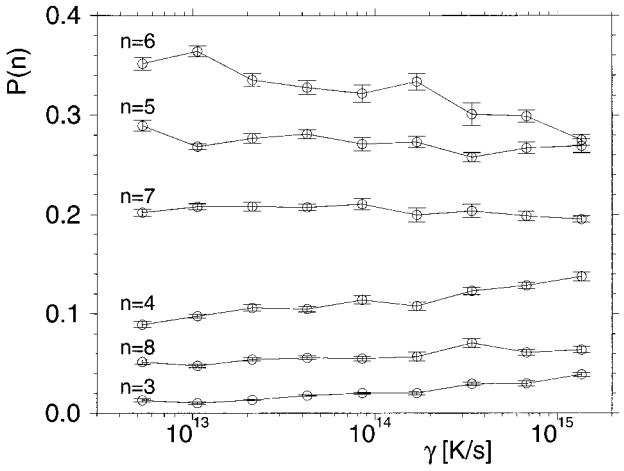

FIG. 14. Probability that a particle is a member of a ring of size n vs the cooling rate.

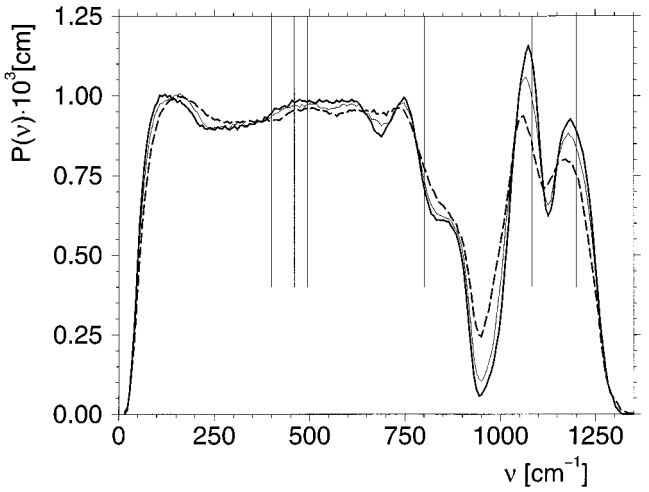

FIG. 15. Spectrum of the system for three different cooling rates: $\gamma = 1.14 \times 10^{15}$ K/s (bold dashed line), $\gamma = 7.10 \times 10^{13}$ K/s, and $\gamma = 4.44 \times 10^{12}$ K/s (bold solid line). The vertical lines give the location of the peaks as determined in the experiments of Refs. 63–65.

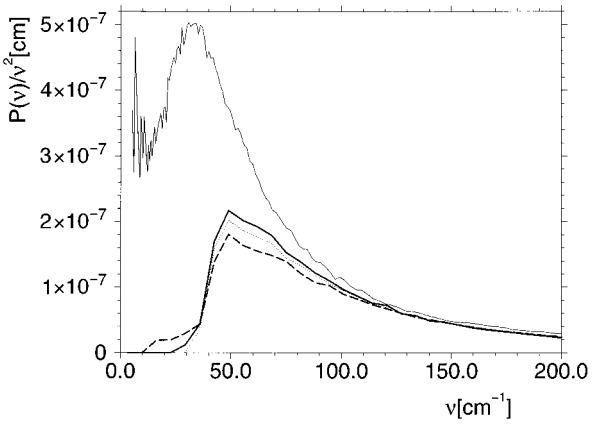

FIG. 16. Density of states divided by ν^2 for three different cooling rates: $\gamma = 1.14 \times 10^{15}$ K/s (bold dashed line), $\gamma = 7.10 \times 10^{13}$ K/s, and $\gamma = 4.44 \times 10^{12}$ K/s (bold solid line). Also included is the result from neutron scattering experiments (Refs. 68 and 70).

Fig. 15 we show the so-obtained spectrum. In order not to crowd the figure too much we present only three of the cooling rates investigated (see figure caption for details). The spectrum of amorphous silica has also been measured in neutron and Raman scattering experiments and it was found that it shows several peaks. Galeener and Lucovsky[63] report lines at 495 and 1200 cm^{-1}, and Kucirková and Navrátil[64] lines at 460, 802, and 1084 cm^{-1} for their Raman scattering experiments, and Carpenter and Price find peaks at 400, 810, 1070, and 1190 cm^{-1} in their neutron scattering experiment.[65] The locations of these peaks are included in the figure as well (vertical lines). We see that the spectrum has two main features. The first one is a double peak at high frequencies and the second one is a broad, relatively featureless mountain at intermediate and low frequencies. It should also be noted that there is a gap at small frequencies which is a finite-size effect, since the acoustic modes with very small frequencies have a wavelength that exceeds the size of the simulation box.

Let us first discuss the double peak at high frequencies. We see that the effect of a decreasing cooling rate is to increase significantly the height of the two peaks as well as to decrease the minimum between the two peaks. Furthermore, we see a small shift of the positions of the two peaks to higher frequencies when the cooling rate is decreased. We recognize that the location of the two peaks reproduces well the ones of the experiment and, because of the mentioned shift, the accordance between experiment and simulation becomes even better with decreasing cooling rate. Note that it is a nontrivial feature of the model that the spectrum shows at high frequencies the double-peak structure observed in experiments. Jin *et al.* have, e.g., found in their simulation of amorphous silica, in which a three-body potential was used, that at high frequencies *three* peaks are present[22] and della Valle and Venuti have shown[23] that the potential proposed by Tsunekuki *et al.*[66] gives two peaks, but that their location does not match the one of the experiments as well as we find it here for the BKS potential. Thus we conclude that with respect to this property the BKS potential seems to be superior to the other potentials investigated so far.

The part of the spectrum at intermediate frequencies shows a relatively weak dependence on the cooling rate. This is not surprising, since most of the modes associated with these frequencies are relatively extended and, since the structure of the system at larger distances is not affected strongly by the cooling rate, these modes are likely not to be affected by the cooling rate either. A more detailed investigation of this point will be published elsewhere.[62]

The spectrum we find at intermediate frequencies seems to reproduce the experimental spectrum less well than the high-frequency part, in that we do not see any prominent feature in the range 400–500 cm^{-1} which is in disagreement with experiments. This is probably due to the fact that in this frequency range most of the modes involve the movement of several particles; thus they extend over a larger region of space. Since it is much harder to devise potentials that are able to reproduce correctly the forces also on the intermediate-range distances, it is not surprising that the BKS potential does not do well on this point and it shares this flaw with the other models as well.[22–25] In passing we also note that the spectrum as determined from a simulation with the original BKS potential, i.e., without the truncation of the short-range part, gives essentially the same spectrum,[67] thus showing that the discrepancy between the experiment and our simulation is not due to this truncation.

The low-frequency part of the spectrum of glassy materials has recently been the focus of interest of several investigations since it was found that in this frequency range there exists an excess of harmonic excitation, the nature of which is still a matter of debate.[68,69] In Fig. 16 we show the low-frequency part of the spectra for three different cooling rates. Since it is customary in experiments to plot not the density of states itself, but the density of states divided by frequency squared, we have done likewise. Also included in the figure is the data from neutron scattering experiments by Buchenau *et al.*[68,70] Note that these curves contain no adjustable parameter. We recognize that qualitatively the results of the experiment and the one of our simulation are quite similar. Furthermore, we see that the agreement between experiment and simulation improves with decreasing cooling rate. Because

of the above-mentioned gap in the density of state, it can, however, be expected that even for a significantly smaller cooling rate the discrepancy between experiment and simulation will not disappear. For this to happen it is likely that one has to investigate system sizes that are significantly larger than the one used here, which is, however, currently too demanding on computer resources.

C. Properties of the system at finite temperatures

Having presented in Sec. III A the cooling-rate dependence of the glass transition and in Sec. III B the cooling-rate dependence of various properties of the glass at zero temperature we use the remaining of this section to investigate the *equilibrium* properties of the system at finite temperatures and to compare these with the ones of the glass. In particular we want to find out at what temperature which properties of the glass are frozen in or, in other words, how the fictive temperature depends on the property. Furthermore, we attempt to understand what the microscopic reason is for the occurrence of the density anomaly.

In order to address these questions we saved some of the configurations of the system during the cooling run with the slowest cooling rate and analyzed these configurations at selected temperatures. In particular we investigated configurations at $T_b = 7000$ K, the highest temperature, at $T_b = 4840$ K, the location of the local maximum in the density, and at $T_b = 3220$ K, the temperature of the local minimum in the density between the temperature of the density maximum and zero temperature (see Fig. 4). In the previous subsection we have concluded that for the smallest cooling rate the glass transition temperature is around 2900 K (see Fig. 2). Thus we expect that the results at the three selected finite temperatures are all equilibrium results, provided that the glass transition temperature does not depend too strongly on the quantity investigated (remember that the glass transition temperatures presented in Fig. 2 are, strictly speaking, only valid for the enthalpy).

The comparison of the structure at finite and zero temperatures was done in two ways. One was to compute for the configurations at finite temperatures the same quantities that we have investigated at zero temperature, such as the radial distribution function, and to compare these quantities with the ones obtained for the glass at zero temperature. The second way was to take these configurations, to determine their intrinsic structure[71] by relaxing the enthalpy via a steepest descent procedure, to compute also for these *relaxed* configurations the quantities that we investigated for the glass, and to compare again. Following Stillinger and Weber we will call in the following the properties of the system (such as, e.g., the density) that are obtained from the relaxed configurations ''intrinsic'' properties (e.g., intrinsic density). Note that doing a steepest descent procedure at $T_b = 7000$ K is equivalent to use an infinitely fast cooling rate. Thus the so-obtained result can also be related to the ones of the previous subsection.

The first quantity we start with is the enthalpy. For the not-relaxed configuration the value of $H(T_b)$ can be read off from Fig. 1. The values of the enthalpy for the relaxed configurations are included in Fig. 6 as horizontal lines. We see that the higher the temperature, the higher the value of the intrinsic enthalpy. At the two highest temperatures, its value is larger than the values obtained from quenches with different cooling rates. This is consistent with the observation that these two temperatures are larger than the glass transition temperatures found for the various cooling rates (see Fig. 2). For the lowest temperature, i.e., $T_b = 3220$ K, the value of the intrinsic enthalpy is about the same as H_f obtained for the cooling rate $\gamma = 3.55 \times 10^{13}$ K/s (see Fig. 6). From Fig. 2 we recognize that for this cooling rate the glass transition temperature is about 3050 K, which is reasonably close to 3220 K, the considered temperature of the system. Thus we find that the temperature of the glass transition, as determined in the way described in Sec. III A, gives a reasonable estimate for the temperature at which the system falls out of equilibrium with respect to the enthalpy as observable.

A similar result is found for the case of the density. In Fig. 7 the horizontal lines give the values of the density of the relaxed configurations at the three temperatures considered. From this graph we recognize that for the two higher temperatures the density is larger than the ones obtained from the quenches with the different cooling rates. Thus this is again in accordance with the observation that the glass transition temperature of these quenches is below these two higher temperatures (see Fig. 2). For the lowest temperature, i.e., 3220 K, the density we find for the relaxed configurations is comparable to the one we found for a quench with a cooling rate in the range 4.44×10^{12} K/s $\leqslant \gamma \leqslant 3.55 \times 10^{13}$ K/s, which corresponds to a range of glass transition temperatures (see Fig. 2) of 2900 K $\leqslant T_g \leqslant$ 3050 K. Thus also in the case of the density the glass temperature is a reasonable estimate for the temperature at which the system falls out of equilibrium.

From Fig. 7 we also recognize that, to within the error bars, the intrinsic density at 7000 and 4840 K is the same. Furthermore, we see that when the temperature is lowered to 3220 K, the intrinsic density changes relatively strong and then remains almost constant when the temperature is lowered further (as can be recognized from the fact that ρ_f depends only weakly on γ, when the cooling rate is not too large, even though the corresponding glass transition temperature is still decreasing in this range of γ). Thus we conclude that the intrinsic density can be considered to be essentially constant for temperatures above 4840 K, the location of the anomaly in the density, and below 3220 K, the location of the local minimum of the density, and that the intrinsic density changes mainly in the temperature range between the local maximum and the local minimum of the density. Note that this temperature dependence of the *intrinsic* density is in stark contrast with the one of the density. For the latter we find that it is changing at all temperatures and that it shows a local maximum and a local minimum whereas the temperature dependence of the former seems to be much simpler. Thus it seems that the intrinsic structure of the network changes mainly in the temperature interval between the mentioned maximum and minimum.

In order to study this effect in more detail we investigate the radial distribution function $g(r)$. In Fig. 17 we show this quantity for the Si-O correlation without the relaxation [Fig. 17(a)] and after the relaxation [Fig. 17(b)]. Also included are the curves we obtained from the quench with the smallest cooling rate (curves labeled with $T = 0$ K). From panel (a)

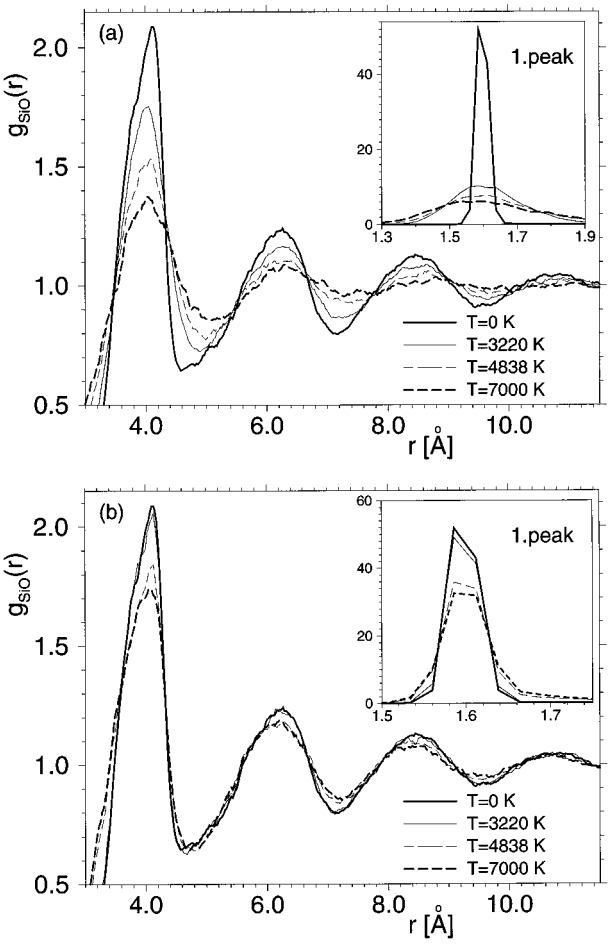

FIG. 17. Radial distribution function $g(r)$ for the Si-O correlation at $T_b=7000$ K, $T_b=4840$ K, and $T_b=3220$ K. Also included is the $g(r)$ as obtained from quenching the system to $T=0$ K with the smallest cooling rate. (a) Without relaxation. (b) With relaxation.

we recognize that $g(r)$ depends quite strongly on the temperature in that the height of the individual peaks and minima become more pronounced. This effect is most prominent for the first-nearest-neighbor peak [inset of Fig. 17(a)]. This change with temperature takes place throughout the whole temperature range investigated. This is not the case with the intrinsic $g(r)$ [panel (b)]. We see that in this case the curves corresponding to $T_b=7000$ K and $T_b=4840$ K are almost the same. They differ, however, significantly from the curve at $T_b=3220$ K, which in turn is very similar to the curve for $T=0$ K. Thus, as in the case of the density, we come also here to the conclusion that the intrinsic structure of the network is changing mainly in the temperature range between the local maximum and the local minimum of the density. Similar results were found for the *intrinsic* radial distribution functions for Si-Si and O-O,[27] and thus we will not show these functions here.

Equipped with the radial distribution functions we can identify the nearest neighbors of every particle via the location of the first minimum in the radial distribution function at the corresponding temperature. The values for $r_{\min}^{\alpha\beta}$ at finite temperatures are given in Table III. As in the case of the radial distribution function we find that these distribution functions show a relatively regular dependence on temperature.[27] An exception, however, seems to be the distribution function for the O-O pairs. We find that this distribution function depends only weakly on temperature for $T\leqslant 3220$ K but then changes strongly when the temperature is lowered to $T=0$ K in that it shifts its maximum from $z=8$ to $z=6$ and becomes peaked much stronger. The reason for this is likely to be the opening of the network with decreasing temperature. However, why this change is so pronounced and why it takes place in the temperature range below 3220 K and not as the other quantities in the temperature range 3220 K $\leqslant T\leqslant 4840$ K is unclear.

TABLE III. Location of the first minimum in the radial distribution function $g(r)$.

T_b	$r_{\min}^{\mathrm{SiSi}}$ [Å]	$r_{\min}^{\mathrm{SiO}}$ [Å]	$r_{\min}^{\mathrm{OO}}$ [Å]
7000 K	3.80	2.50	3.70
4838 K	3.37	2.50	3.60
3220 K	3.37	2.30	3.25

The distribution functions for the intrinsic coordination numbers show the usual dependence on temperature in that they show only a weak temperature dependence for $T\leqslant 3220$ K and $T\geqslant 4840$ K, and a much stronger dependence in the temperature range 3220 K $\leqslant T\leqslant 4840$ K. Thus also for these quantities the relevant changes take place in the temperature range between the local maximum and the local minimum in the density.

The changing of the structure of the network can also be studied well with the help of the angles between the various atoms, which are shown in Fig. 18. The distributions of the intrinsic angles at $T_b=4840$ K and at $T_b=3220$ K are very similar to the ones at $T_b=7000$ K and $T=0$ K, respectively.[27] Thus also in this case the intrinsic structure is essentially independent of temperature for T higher than 4840 K and for temperatures lower than 3220 K. Only in the temperature range 3220 K $\leqslant T\leqslant 4840$ K does the distribution of the intrinsic angles change significantly. In contrast to this we see that the distribution of the angles, i.e., without the relaxation, depends on T for the whole temperature range. In particular we find [see Fig. 18(a)], that the distribution for the angle O-Si-O is very broad at high temperatures and becomes gradually narrower when T is decreased. Thus we find that the tetrahedra are significantly distorted at high temperature, in accordance with the observation that the first-nearest-neighbor peak in $g_{\mathrm{SiO}}(r)$ becomes relatively broad at high temperatures [see Fig. 17(a)].

Also the distribution of the angle Si-O-Si changes significantly with temperature, Fig. 18(b). The position of the large peak that is present at $T=0$ K moves to smaller angles and becomes much broader when the temperature increases. Since this angle measures the relative orientation between two neighboring tetrahedra, this observation is in accordance with the picture of the densifying network, when the temperature is increased. The same conclusion can be drawn from the distribution of the O-O-O angle, shown in Fig. 18(c). The position of the broad secondary peak, corresponding to the angle between an oxygen atom on one tetrahedron, a bridging oxygen, and an oxygen on a second tetrahedron (O#1-O#3-O#2 in Fig. 11), moves to smaller angles with increasing temperature, indicating that the two tetrahedra

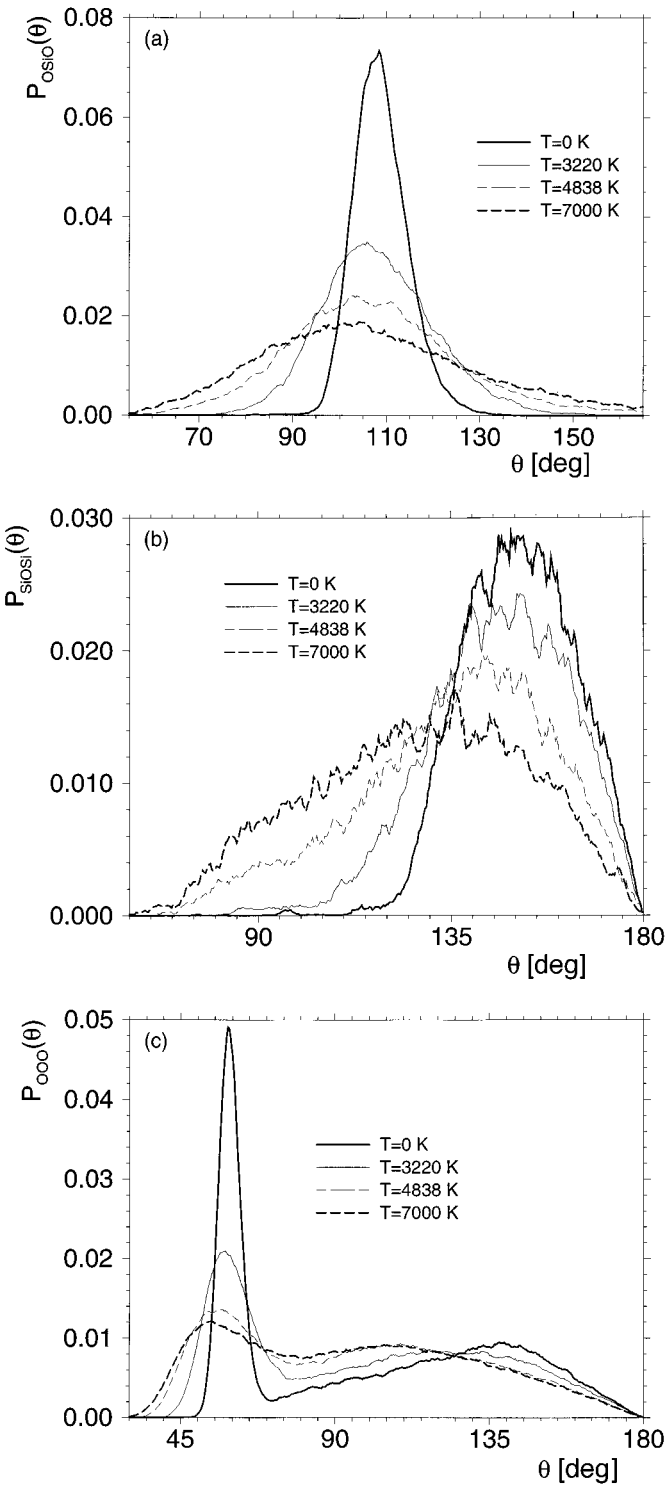

FIG. 18. Distribution function for various angles at $T_b = 7000$ K, $T_b = 4840$ K, and $T_b = 3220$ K (without relaxation). Also included is the distribution function as obtained from quenching the system to $T = 0$ K with the smallest cooling rate. (a) O-Si-O. (b) Si-O-Si. (c) O-O-O.

move closer to each other. At the same time the main peak, corresponding to the angle of three oxygen atoms on the same tetrahedron, decreases its height and becomes broader, showing that the tetrahedra are more distorted at high temperatures.

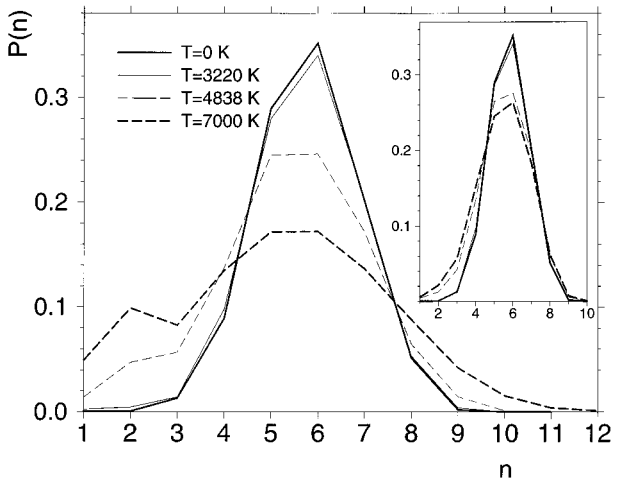

FIG. 19. Distribution of the size of the rings at $T_b = 7000$ K, $T_b = 4840$ K, and $T_b = 3220$ K. Also included is the distribution function as obtained from quenching the system to $T = 0$ K with the smallest cooling rate. Main figure: without relaxation. Inset: with relaxation.

The last structural quantity we investigate is the distribution of the size of the rings which is shown in Fig. 19. We see that also in this case the distribution of the intrinsic size of the rings (see the inset of Fig. 19) depends significantly on the temperature only in the temperature range 3220 K $\leqslant T \leqslant$ 4840 K. The distribution function of the ring size without the relaxation shows, however, a temperature dependence that extends throughout the whole temperature range investigated. We see that this distribution becomes significantly broader when the temperature is increased and that the main change is that the short rings become more frequent. We also note that at high temperatures we find some ''rings'' that have a size $n = 1$, by which we denote ''rings'' that are not closed, i.e., which are dangling bonds. These types of rings disappear when the temperature is less than 4840 K, showing that from an energetic point of view such configurations are unfavorable.

The final quantity we studied was the spectrum of the system, which is shown in Fig. 20. The intrinsic spectrum, shown in Fig. 20(a), shows that the main effect of finite temperature is to smear out the double-peak structure at high frequencies and to fill up the gap between this double-peak structure and the broad mountain at lower frequencies. The main change in the form of the spectrum takes again place in the temperature interval 3220 K $\leqslant T_b \leqslant$ 4840 K.

The spectrum at finite temperature is quite different from the intrinsic one, since the dynamical matrix has also negative eigenvalues. It is customary to plot the distribution of the square root of these negative eigenvalues on the negative frequency axis.[61] We see that at finite temperatures the double peak at high frequencies is reduced to a shoulder of the large mountain at lower frequencies. This is the case even for $T_b = 3220$ K, i.e., the temperature for which we have found that most structural properties of the system are very similar to the ones at $T = 0$ K. Thus we find that this dynamic quantity shows a much stronger temperature dependence at low temperatures than the structural quantities. The peak in the distribution at negative frequencies, however,

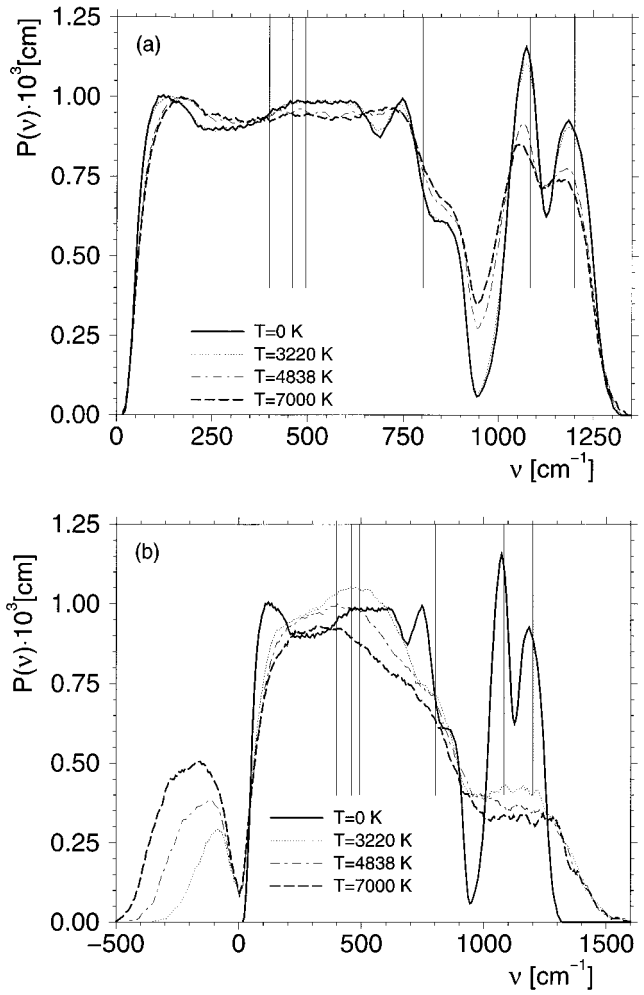

FIG. 20. Spectrum of the system at $T_b = 7000$ K, $T_b = 4840$ K, and $T_b = 3220$ K. Also included is the spectrum as obtained from quenching the system to $T = 0$ K with the smallest cooling rate. The vertical lines gives the location of the peaks as determined in the experiment of Refs. 63–65. (a) With relaxation. (b) Without relaxation. The distribution for negative frequencies corresponds to negative eigenvalues of the dynamical matrix.

shows a regular dependence on temperature, thus being more similar to the structural quantities.

IV. SUMMARY AND CONCLUSIONS

We have presented the results of a large scale computer simulation in which we investigated how the properties of silica glass depend on the cooling rate with which the glass was produced. Experiments in which such cooling rate dependences were investigated have focused, so far, only on the *macroscopic* properties of glasses, such as the density or the glass transition temperature.[72] One of the main goals of our investigation was to study how the *microscopic* properties of the glass are affected by the cooling rate and see how their cooling-rate dependence compares with the one of macroscopic properties. The second goal of our study was to test whether the silica potential proposed by van Beest, Kramer, and van Santen (BKS), which so far has only been used to describe crystalline and pressurized amorphous silica, is also suitable to model vitreous silica produced via a quench in temperature.

In our work we first focused on the macroscopic quantities, in order to see whether the cooling-rate dependence of these quantities show a similar behavior as the ones observed in real experiments. We found that this is indeed the case, in that, e.g., the dependence of the glass transition temperature on the cooling rate is in qualitative accordance with the one of real materials. If this observed cooling-rate dependence is extrapolated to experimental cooling rates, this accordance seems also to be correct in a semiquantitative way.

We also observed that, if the cooling rate is sufficiently small, the density shows an anomalous behavior in that it has a maximum at around 4800 K. Such an anomaly is also found in real silica, although at a significantly smaller temperature (1820 K). This shows that with respect to this phenomenon the BKS potential is able to give at least a qualitatively correct description of noncrystalline silica.

By investigating the properties of the glass at zero temperature we find that the enthalpy, the density, and the thermal expansion coefficient depend significantly on the cooling rate. The densities we find are in agreement with the ones of real silica and an extrapolation of the thermal expansion coefficient to experimental cooling rates is also consistent with the experimental values for this quantity. Thus we find also in this case that the BKS potential is a good model for real silica glass.

After having made sure that the BKS potential gives a reasonably good description of the *macroscopic* properties of amorphous silica and that our simulations are able to reproduce the cooling-rate dependence of the glass transition at least in a qualitative way we thus could move on to investigate how the *microscopic* properties of the glass depend on the cooling rate. We found that the radial distribution functions showed a pronounced dependence on the cooling rate in that the individual peaks become significantly more pronounced with decreasing cooling rate. From this and the fact that the first sharp diffraction peak in the structure factor also shows a significant cooling-rate dependence towards becoming more pronounced with decreasing cooling rate, we conclude that the structure of the system at short and intermediate distances becomes more ordered. This conclusion is also corroborated by our observation that the distribution of the bond angles becomes more structured and that the various coordination numbers show the tendency that the basic units in the network become more ideal, i.e., to become regular tetrahedra. That also the intermediate-range order of the glass increases with decreasing cooling rate can also be inferred from the observation that in the distribution of the size of the rings the frequency of rings of size 6 increases with decreasing cooling rate, which shows that the *local* structure of the system approaches the one of β-cristobalite.

Also the spectrum of the system, as computed from the eigenvalues of the dynamical matrix, shows a noticeable dependence on the cooling rate in that the two main peaks at high frequencies become more pronounced when γ is lowered. This shows that the neighborhoods of the individual atoms show less variation from atom to atom with decreasing cooling rate. In addition we find that the location of these two peaks is very close to the one observed in experiments, demonstrating that the BKS potential is reliable with respect

to this quantity as well. Furthermore, we have shown that also at low frequencies the spectrum is in fair agreement with experiment.

Finally we investigated how the structure of the glass at finite temperatures differs from the one at zero temperature in order to find out how the glass transition is affecting the temperature dependence of various quantities. We find that the radial distribution functions show a smooth dependence on temperature, thus showing that the glass transition is not accompanied by a dramatic change in this quantity. This is the case for most other structural quantities considered. However, if we look at the *intrinsic* quantities, we note that they show a much more pronounced temperature dependence. Roughly speaking we can say that above and below the glass transition the intrinsic quantities are essentially independent of temperature, that they change, however, significantly in the vicinity of the glass transition. This shows that these quantities are likely to be a sensitive indicator for when the system is undergoing the glass transition in accordance with the findings of Stillinger and Weber[71] and Jónsson and Andersen.[73]

From the temperature dependence of the various structural quantities we gain some understanding on the nature of the density anomaly. We find that the network becomes more compact when the temperature is lowered from high temperatures to 4800 K, the temperature at which the anomaly is observed. This shrinking is a complicated process in which certain distances increase, whereas others decrease and where also the distribution of the various angles changes significantly with temperature. When the temperature is decreased even further the density decreases again which can be understood from a microscopic point of view by a change in the distribution of the various angles which lead to an opening up of the network. The nearest-neighbor bond distances, however, do not change significantly in this temperature range, showing that the relative positions of the tetrahedra among each other are more important for the anomaly than the geometry of the tetrahedra.

To conclude we can say that we have shown that, similar to fragile glass formers,[14] also the properties of strong glasses show a noticable dependence on the cooling rate with which the glass was produced. In particular we showed that such dependences can affect the microscopic quantities much more than they affect the macroscopic ones and that it might therefore also be interesting to investigate in real experiments how microscopic quantities depend on the cooling rate. In addition we have shown that the two-body potential proposed by van Beest *et al.* for crystalline silica is also able to give a surprisingly good description of amorphous silica, thus making it possible to investigate these types of glasses in a relatively efficient manner.

ACKNOWLEDGMENTS

We thank C. A. Angell for valuable discussions, U. Buchenau for permitting us to reproduce his data before publication, and S. Klaumünzer for informing us on experiments on ion bombardment. K. V. thanks Schott-Glaswerke Mainz for financial support through the Schott-Glaswerke-Fond and the DFG, through SFB 262, for financial support. Part of this work was done on the computer facilities of the Regionales Rechenzentrum Kaiserslautern.

*Present address: Institute for Physical Science and Technology University of Maryland, College Park, Maryland 20742. Electronic address: vollmayr@ipst.umd.edu

†Author to whom correspondence should be addressed. Electronic address: kob@moses.physik.uni-mainz.de
http://www.cond-mat.physik.uni-mainz.de/~kob/home_kob.html

[1] C. A. Angell, J. H. R. Clarke, and L. V. Woodcock, Adv. Chem. Phys. **48**, 397 (1981).

[2] J.-L. Barrat and M. L. Klein, Annu. Rev. Phys. Chem. **42**, 23 (1991).

[3] W. Kob, in *Annual Reviews of Computational Physics*, edited by D. Stauffer (World Scientific, Singapore, 1995), Vol. III, p. 1.

[4] See, e.g., W. Götze and L. Sjögren, Rep. Prog. Phys. **55**, 241 (1992); for an up-to-date list of references related to mode-coupling theory see W. Kob and H. C. Andersen, Phys. Rev. E **51**, 4626 (1995).

[5] H. N. Ritland, J. Am. Ceram. Soc. **37**, 370 (1954).

[6] See, e.g., C. Y. Yang, D. E. Sayers, and M. A. Paesler, Phys. Rev. B **36**, 8122 (1987); C. T. Limbach and U. Gonser, J. Non-Cryst. Solids **106**, 399 (1988); G. P. Johari, A. Hallbrucker, and E. Mayer, J. Phys. Chem. **93**, 2648 (1989); B. J. Zappel and F. Sommer, J. Non-Cryst. Solids (to be published).

[7] R. Brüning and K. Samwer, Phys. Rev. B **46**, 11 318 (1992).

[8] R. Brüning and M. Sutton, Phys. Rev. B **49**, 3124 (1994).

[9] J. R. Fox and H. C. Andersen, J. Phys. Chem. **88**, 4019 (1984).

[10] H. Miyagawa and Y. Hiwatari, Phys. Rev. A **40**, 6007 (1989); S. K. Lai and M. S. Lin, J. Non-Cryst. Solids **117/118**, 907 (1990); R. Speedy, Mol. Phys. **83**, 591 (1994).

[11] J. Baschnagel, K. Binder, and H.-P. Wittmann, J. Phys. Condens. Matter **5**, 1597 (1993).

[12] K. Vollmayr, W. Kob, and K. Binder, in *Computer Simulation Studies in Condensed Matter Physics VIII*, edited by D. P. Landau, K. K. Mon, and H. B. Schüttler (Springer, Berlin, 1995), p. 117.

[13] K. Vollmayr, W. Kob, and K. Binder, Europhysics Lett. **32**, 715 (1995).

[14] K. Vollmayr, W. Kob, and K. Binder, J. Chem. Phys. **105**, 4714 (1996).

[15] See, e.g., S. Klaumünzer, Mater. Sci. Forum **97-99**, 623 (1992) and references therein.

[16] B. W. H. van Beest, G. J. Kramer, and R. A. van Santen, Phys. Rev. Lett. **64**, 1955 (1990).

[17] See, e.g., S. K. Mitra, M. Amini, D. Fincham, and R. W. Hockney, Philos. Mag. B **43**, 365 (1981); S. H. Garofalini, J. Chem. Phys. **76**, 3189 (1982); R. L. Erikson and C. J. Hostetler, Geochim. Cosmochim. Acta **51**, 1209 (1987); B. P. Feuston and S. H. Garofalini, J. Chem. Phys. **89**, 5818 (1988); J. D. Kubicki and A. C. Lasaga, Am. Mineral. **73**, 941 (1988); B. Vessal, M. Lesslie, and C. R. A. Catlow, Mol. Sim. **3**, 123 (1989); P. Vashishta, R. K. Kalia, J. P. Rino, and I. Ebbsjö, Phys. Rev. B **41**, 12 197 (1990); R. G. della Valle and H. C. Andersen, J. Chem. Phys. **94**, 5056 (1991); **97**, 2682 (1992); M. S. Somayazulu, S. M. Sharma, N. Garg, S. L. Chaplot, and S. K. Sikka, J. Phys. Condens. Matter **5**, 6345 (1993); N. Binggeli, J. R. Chelikowski, and R. M. Wentzcovitch, Phys. Rev. B **49**, 9336 (1994); W. Jin, R. K. Kalia, P. Vashishta, and J. P. Rino, *ibid.* **50**, 118 (1994); J.

Sarntheim, A. Pasquarello, and R. Car, Phys. Rev. Lett. **74**, 4682 (1995).
[18] J. Kieffer and C. A. Angell, J. Chem. Phys. **90**, 4982 (1989).
[19] T. F. Soules, J. Non-Cryst. Solids. **73**, 315 (1985); S. K. Mitra, Philos. Mag. B **47**, L63 (1983); B. Vessal, M. Amini, D. Fincham, and C. R. A. Catlow, *ibid.* **60**, 753 (1989).
[20] J. P. Rino, I. Ebbsjö, R. K. Kalia, A. Nakano, and P. Vashishta, Phys. Rev. B **47**, 3053 (1993).
[21] J. Badro, J.-L. Barrat, and P. Gillet, Phys. Rev. Lett. **76**, 772 (1996).
[22] W. Jin, P. Vashishta, R. K. Kalia, and J. P. Rino, Phys. Rev. B **48**, 9359 (1993).
[23] R. G. della Valle and E. Venuti, Chem. Phys. **179**, 411 (1994).
[24] S. K. Mitra, Philos. Mag. B **45**, 529 (1982).
[25] S. H. Garofalini, J. Non-Cryst. Solids **63**, 337 (1984).
[26] K. Vollmayr and W. Kob, Ber. Bunsenges. Phys. Chem. **100**, 1399 (1996).
[27] K. Vollmayr, Ph.D. thesis, Universität Mainz, 1995.
[28] J. S. Tse and D. D. Klug, Phys. Rev. Lett. **67**, 3559 (1991); J. Chem. Phys. **95**, 9176 (1991); J. S. Tse, D. D. Klug, and Y. Le Page, Phys. Rev. B **46**, 5933 (1992); Phys. Rev. Lett. **69**, 3647 (1992); J. S. Tse, D. D. Klug, and D. C. Allan, Phys. Rev. B **51**, 16 392 (1995).
[29] M. P. Allen and D. J. Tildesley, *Computer Simulation of Liquids* (Oxford University Press, New York, 1990).
[30] H. C. Andersen, J. Chem. Phys. **72**, 2384 (1980); see also Ref. 9.
[31] W. H. Press, S. A. Teukolsky, W. T. Vetterling, and B. P. Flannery, *Numerical Recipes in Fortran*, 2nd ed. (Cambridge University Press, Cambridge, England, 1992).
[32] A. Q. Tool and C. G. Eichlin, J. Opt. Soc. Am. **14**, 276 (1931).
[33] C. A. Angell and L. M. Torell, J. Chem. Phys. **78**, 937 (1983).
[34] C. A. Angell, J. Chem. Phys. Solids **49**, 863 (1988).
[35] See, e.g., K. Hofer, E. Mayer, and G. P. Johari, J. Phys. Chem. **95**, 7100 (1991); C. L. Jackson and G. B. McKenna, J. Non-Cryst. Solids **131-133**, 221 (1991); J. Zhang, G. Liu, and J. Jonas, J. Phys. Chem. **96**, 3478 (1992); P. Pissis, D. Daoukaki-Diamanti, L. Apekis, and C. Christodoulides, J. Phys. Condens. Matter **6**, L325 (1994); J. Schüller, Y. B. Mel'nichenko, R. Richert, and E. W. Fischer, Phys. Rev. Lett. **73**, 2224 (1994); T. Fehr and H. Löwen, Phys. Rev. E **52**, 4016 (1995).
[36] J. L. Horbach, W. Kob, K. Binder, and C. A. Angell, Phys. Rev. E (to be published).
[37] E. Rössler and A. P. Sokolov, Chem. Geol. **128**, 143 (1996).
[38] C. A. Angell, J. Phys. Chem. **97**, 6339 (1993).
[39] C. H. Reinsch, Num. Math. **10**, 177 (1967); **16**, 451 (1971).
[40] R. Brückner, J. Non-Cryst. Solids **5**, 123 (1970).
[41] O. V. Mazurin, M. V. Streltsina, and T. P. Shvaiko-Shvaikovskaya, *Handbook of Glass Data* (Elsevier, Amsterdam, 1983), Pt. A.
[42] The pressure dependence of the location of the maximum in the density was investigated in C. A. Angell and H. Kanno, Science **179**, 1121 (1976).
[43] R. L. Mozzi and B. E. Warren, J. Appl. Cryst. **2**, 164 (1969).
[44] J.-L. Barrat (private communication).
[45] *Handbook of Chemistry and Physics*, 65th ed., edited by R. C. Weast, M. J. Astle, and W. H. Beyer (The Chemical Rubber Co., Boca Raton, 1984).
[46] W. Kob and R. Schilling, J. Phys. A **23**, 4673 (1990) and references therein.
[47] G. S. Grest, C. M. Soukoulis, and K. Levin, Phys. Rev. Lett. **56**, 1148 (1986); G. S. Grest, C. M. Soukoulis, K. Levin, and R. E. Randelman, in *Heidelberg Colloquium on Glassy Dynamics*, Vol. 275 of *Lecture Notes in Physics*, edited by J. L. van Hemmen and I. Morgenstern (Springer, Berlin, 1987), p. 307; D. A. Huse and D. S. Fisher, Phys. Rev. Lett. **57**, 2203 (1986).
[48] S. Cornell, K. Kaski, and R. B. Stinchcombe, J. Phys. A **24**, L865 (1991); J. Jäckle, R. B. Stinchcombe, and S. Cornell, J. Stat. Phys. **62**, 425 (1991); S. Shinomoto and Y. Kabashima, J. Phys. A **24**, L141 (1991); P. Sibani, J. M. Pedersen, K. H. Hoffmann, and P. Salamon, Phys. Rev. A **42**, 7080 (1990).
[49] J.-P. Hansen and I. R. McDonald, *Theory of Simple Liquids* (Academic, London, 1986).
[50] D. I. Grimley, A. C. Wright, and R. N. Sinclair, J. Non-Cryst. Solids **119**, 49 (1990).
[51] J. H. Konnert and J. Karle, Acta Crystallogr. A **29**, 702 (1973).
[52] See, e.g., S. Susman, K. J. Volin, D. L. Price, M. Grimsditch, J. P. Rino, R. K. Kalia, and P. Vashishta, Phys. Rev. B **43**, 1194 (1991); S. R. Elliott, J. Non-Cryst. Solids **150**, 112 (1992); J. H. Lee and S. R. Elliott, Phys. Rev. B **50**, 5981 (1994); E. A. Chechetkina, J. Phys. Condens. Matter **7**, 3099 (1995); F. J. Bermejo, M. Garcia-Hernández, F. J. Mompeán, D. MacMorrow, and J. L. Martinez, Phys. Rev. B **51**, 11 932 (1995); P. H. Gaskell and D. J. Wallis, Phys. Rev. Lett. **76**, 66 (1996); F. J. Bermejo, J. Dawidowski, R. Fernández-Perea, and J. L. Martinez, Phys. Rev. B **54**, 244 (1996).
[53] See, e.g., R. Zallen, *Physics of Amorphous Solids* (John Wiley and Sons, New York, 1983).
[54] R. F. Pettifer, R. Dupree, I. Farnan, and U. Sternberg, J. Non-Cryst. Solids **106**, 408 (1988).
[55] P. G. Coombs, J. F. De Natale, P. J. Hood, E. K. McElfresh, R. S. Wortman, and J. F. Schackelford, Philos. Mag. **51**, L39 (1985).
[56] J. R. G. Da Silva, D. G. Pinatti, C. E. Anderson, and M. L. Rudee, Philos. Mag. **31**, 713 (1975).
[57] D. Stöffler and J. Arndt, Naturwissenschaften **56**, 100 (1969).
[58] R. J. Bell and P. Dean, Trans. Faraday Soc. **50**, 55 (1970); R. Biswas, A. M. Bouchard, W. A. Kamitakahara, G. S. Grest, and C. M. Soukoulis, Phys. Rev. Lett. **60**, 2280 (1988).
[59] B. B. Laird and H. R. Schober, Phys. Rev. Lett. **66**, 636 (1991); H. R. Schober and B. B. Laird, Phys. Rev. B **44**, 6746 (1991).
[60] N. G. Almarza, E. Enciso, and F. J. Bermejo, J. Chem. Phys. **99**, 6876 (1993); M. Garcia-Hernandez, F. J. Bermejo, B. Fåk, J. L. Martinez, E. Enciso, N. G. Almarza, and A. Criado, Phys. Rev. B **48**, 149 (1993); C. Oligschleger and H. R. Schober, Physica A **201**, 391 (1993); H. R. Schober, C. Oligschleger, and B. B. Laird, J. Non-Cryst. Solids **156-158**, 965 (1993); H. R. Schober and C. Oligschleger, Nukleonika **39**, 185 (1994); C. Oligschleger, Ph.D. thesis, Jülich, 1994; B. M. Forrest, E. Leontidis, and U. W. Suter, J. Chem. Phys. **104**, 2401 (1996); H. R. Schober and C. Oligschleger (unpublished).
[61] S. D. Bembenek and B. B. Laird, Phys. Rev. Lett. **74**, 936 (1995).
[62] K. Vollmayr and W. Kob (unpublished).
[63] F. J. Galeener and G. Lucovsky, Phys. Rev. Lett. **37**, 1474 (1976).
[64] A. Kucirková and K. Navrátil, Appl. Spectrosc. **48**, 113 (1994).
[65] J. M. Carpenter and D. L. Price, Phys. Rev. Lett. **54**, 441 (1985); D. L. Price and J. M. Carpenter, J. Non-Cryst. Solids **92**, 153 (1987).
[66] S. Tsuneyuki, M. Tsukada, H. Aoki, and Y. Matsui, Phys. Rev. Lett. **61**, 869 (1988).
[67] J. Badro (private communication).
[68] U. Buchenau, M. Prager, N. Nücker, A. J. Dianoux, N. Ahmad, and W. A. Phillips, Phys. Rev. B. **34**, 5665 (1986).
[69] See, e.g., E. Rössler, A. P. Sokolov, A. Kisliuk, and D. Quitmann,

Phys. Rev. B **49**, 14 967 (1994) and references therein; *Dynamics of Disordered Materials*, edited by D. Richter, A. J. Dianoux, W. Petry, and J. Teixeira (Springer, Berlin, 1989); *Proceedings of the Second International Discussion Meeting on Relaxation in Complex Systems* [J. Non-Cryst. Solids **172-174** (1994)].

[70] A. Wischnewski, A. J. Dianoux, and U. Buchenau (unpublished).

[71] F. H. Stillinger and T. A. Weber, J. Chem. Phys. **80**, 4434 (1984); T. A. Weber and F. H. Stillinger, Phys. Rev. B **32**, 5402 (1985).

[72] An exception is a Raman study in which it was found that the intensity of a peak corresponding to a ring of size 3 depends on the cooling rate [B. Champagnon (private communication)].

[73] H. Jónsson and H. C. Andersen, Phys. Rev. Lett. **60**, 2295 (1988).